Regulation of potassium homeostasis in Caulobacter crescentus

Quintero Yanes, Alex Armando; Leger, Loic; Collignon, Madeline; Mignon, Julien; Mayard, Aurelie; Michaux, Catherine; Hallez, Regis

Published in:
bioRxiv

DOI:
https://doi.org/10.1101/2023.07.05.547876

Publication date:
2023

Document Version
Other version

Regulation of potassium homeostasis in *Caulobacter crescentus*

Alex Quintero-Yanes[1+], Madeline Collignon[1], Loïc Léger[1], Aurélie Mayard[1], Régis Hallez[1,2,$,#]

[1]*Bacterial Cell cycle & Development (BCcD), Biology of Microorganisms Research Unit (URBM), Namur Research Institute for Life Science (NARILIS), University of Namur, Namur (5000), Belgium.*

[2]*WELBIO, University of Namur, Namur (5000), Belgium*

[+] *ORCID ID: 0000-0002-8350-0881*

[$] *ORCID ID: 0000-0003-1175-8565*

[#]Corresponding author: Tel: +32 81 724 244; E-mail: regis.hallez@unamur.be

Short title: Potassium homeostasis in *C. crescentus*.

Key words: Potassium transport, two-component system, Kup, KdpE, KdpD

Abstract

Potassium (K^+) is an essential physiological element determining membrane potential, intracellular pH, osmotic/turgor pressure, and protein synthesis in cells. Nevertheless, K^+ homeostasis remains poorly studied in bacteria. Here we describe the regulation of potassium uptake systems in the oligotrophic α-proteobacterium *Caulobacter crescentus* known as a model for asymmetric cell division. We show that *C. crescentus* can grow in concentrations from the micromolar to the millimolar range by essentially using two K^+ transporters to maintain potassium homeostasis, the low affinity Kup and the high affinity Kdp uptake systems. When K^+ is not limiting, we found that the *kup* gene is essential while *kdp* inactivation does not impact the growth. In contrast, *kdp* becomes critical but not essential and *kup* dispensable for growth in K^+-limited environments. However, in the absence of *kdp*, mutations in *kup* were selected to improve growth in K^+-depleted conditions, likely by improving the affinity of Kup for K^+. In addition, mutations in the KdpDE two-component system, which regulates *kdpABC* expression, suggest that the inner membrane sensor regulatory component KdpD works as a kinase in early stages of growth and as a phosphatase to regulate transition into stationary phase. Our data also show that KdpE is not only phosphorylated by KdpD but also by another non-cognate histidine kinase. On top of this, we determined the KdpE-dependent and independent K^+ transcriptome as well as the direct targets of KdpE. Together, our work illustrates how an oligotrophic bacterium responds to fluctuation in K^+ availability.

Introduction

Potassium (K^+) is the most abundant monovalent cation within living cells (Danchin & Nikel, 2019, Epstein, 2003) and it is essential to set the membrane potential and intracellular pH (Bakker & Mangerich, 1981, Booth, 1999, Epstein, 2003, Ochrombel *et al.*, 2011). As K^+ also emerges as an important regulator of bacterial physiology in view of its role in diverse processes (Castaneda-Garcia *et al.*, 2011, Dominguez-Ferreras *et al.*, 2009, Feng *et al.*, 2022, Gries *et al.*, 2013, Humphries *et al.*, 2017, Liu *et al.*, 2013, MacGilvary *et al.*, 2019, Prindle *et al.*, 2015, Quintero-Yanes *et al.*, 2019, Rasmussen, 2023, Su *et al.*, 2009, Valente & Xavier, 2016) including biofilm formation, chemotaxis, cell to cell communication or virulence, it is therefore expected that K^+ transport is tightly regulated.

In bacteria, the KdpDE two-component system (TCS) responds to potassium depletion by regulating the expression of the cognate high-affinity K^+ transporter KdpFABC (Pedersen *et al.*, 2019). This inner membrane complex consists of four subunits all encoded in the same operon, often together with the *kdpDE* genes (Ali *et al.*, 2017, Dani *et al.*, 2017). In *Escherichia coli*, KdpD was shown to act as a dual sensor for K^+, which independently regulates both enzymatic activities. Whereas the kinase activity was inhibited by extracellular K^+, phosphatase activity was stimulated by intracellular K^+ (Schramke *et al.*, 2016). This ultimately determines the phosphorylation status of the response regulator KdpE and thus provides a tight regulation of *kdpFABC* expression and as well as a robust homeostasis in fluctuating environments (Schramke *et al.*, 2016).

Other K^+ transporters have been described in detail in Gram-negative bacteria, such as the inner membrane low-affinity Trk and Kup systems for uptake, and the KefB efflux

63 pump. The Trk potassium uptake system is highly conserved in bacteria and works in
64 a multi-subunit complex comprising the TrkG/H, TrkA and TrkE proteins. TrkH (an extra
65 copy known as TrkG is found in *E. coli*) is the trans-membrane transporter unit, which
66 interacts with the NAD^+- and NADH-binding peripheral protein TrkA and the ATP-
67 binding protein TrkE in the cytoplasmic leaflet to control extracellular potassium uptake
68 when high extracellular concentrations of K^+ are available (Bossemeyer *et al.*, 1989a,
69 Dosch *et al.*, 1991, Harms *et al.*, 2001). On the other hand, Kup is a single protein,
70 constitutively expressed and thought to function as K^+/Na^+ symporter (Dosch *et al.*,
71 1991, Schleyer & Bakker, 1993, Zakharyan & Trchounian, 2001).
72 Recently, it was reported that glutathione controls cell division via negative regulation
73 of KefB in the Gram-negative oligotrophic α-proteobacterium *Caulobacter crescentus*
74 (3). Indeed, mutants unable to synthesize glutathione led to cell filamentation and
75 decreased intracellular K^+ levels. Interestingly, these phenotypes were suppressed by
76 mutations in the KefB efflux pump, suggesting that K^+ homeostasis is crucial for
77 bacterial cell cycle regulation. *C. crescentus* has been extensively used as a model for
78 cell cycle studies since it divides asymmetrically to give birth to a larger sessile stalked
79 cell and a smaller flagellated swarmer cell (1). DNA replication and cell division take
80 place only in sessile stalked cells whereas the swarmer cells remain in a non-
81 replicative but chemotactically active and motile phase able to explore new
82 environments. Once swarmer cells find a suitable – resourceful – habitat for
83 reproduction, they differentiate into stalked cells and concomitantly start DNA
84 replication. In contrast, upon deprivation of environmental resources, the swarmer cells
85 do not differentiate into replicative stalked cells.

In this study, we characterized the response of *Caulobacter* cells grown in environments containing what we defined as limiting, abundant and excessive K^+ concentrations. *In silico* analyses revealed that *C. crescentus* does not have Trk system components but encodes a putative transporter with a cytoplasmic TrkA-like domain. Moreover, in addition to the KefB and KefC efflux pumps, we found genes predicted to code for a Kup and a KdpABC transporters as well as a KdpDE TCS. We generated mutants of these predicted K^+ transporters and assessed their fitness in limiting and abundant K^+ environments. We also characterized the KdpDE system and determined its regulon by ChIP-seq and RNA-seq.

Results

Growth of *C. crescentus* at different K^+ concentrations

To primarily assess the impact of K^+ on *C. crescentus* fitness, the wild-type (WT) strain was grown in K^+-free minimal media (M2G-K) supplemented with K^+ at different concentrations using either KCl or a combination of K_2HPO_4 and KH_2PO_4 (K_2HPO_4 + KH_2PO_4) like the one used in standard M2G minimal media (**Fig. 1**). First, when phosphate salts were used as K^+ source, we observed that compared to M2G, which contains 7 mM K^+, growth started to be significantly impaired at K^+ concentrations below or equal to 0.025 mM and above or equal to 7 mM (**Fig. 1AB**). Second, by using KCl, we found different K^+ concentrations critical for growth since the WT already failed to grow at 0.1 mM but supports growth up to 25 mM (**Fig. 1CD** and **Fig. S1A**). Notwithstanding these differences likely due to the $PO4^{3-}$ and Cl^- counter-anions, the growth of the WT at K^+ concentrations ranging from 0.5 mM to 5 mM was indistinguishable from the one in M2G, that is 7 mM (**Fig. 1**). Therefore, based on these

data, we will use in this study potassium phosphate salts at 0.025 mM and 0.5 mM respectively as limiting and abundant concentrations while KCl will be used at 50 mM as excessive concentration.

K^+ transport and regulation systems in *C. crescentus*

By using *in silico* analyses, we found in the genome of *C. crescentus* NA1000 (NC_011916.1) several genes encoding potential K^+ uptake (*kup* and *kdpABCDE*) or efflux (*kefB*, *kefC* and *kefG*) systems (**Fig. 2**). Although Trk orthologs were not found, a putative transporter (CCNA_01688) containing a cytoplasmic TrkA-like domain was identified (**Fig. 2**). Based on the function of the Kdp, Kef, Kup and Trk systems in other bacteria (Bossemeyer *et al.*, 1989b, Cao *et al.*, 2011, Epstein, 2003, MacGilvary *et al.*, 2019, Roosild *et al.*, 2010), we predicted that transport of K^+ in *C. crescentus* occurs via CCNA_01688, KefBG, KefC and Kup when potassium is abundant in the environment (**Fig. 2A**) whereas the Kdp system might be inactive (**Fig. 2B**) (Heermann & Jung, 2010, Roe *et al.*, 2000). In contrast, K^+-depleted conditions should activate the KdpDE TCS and trigger expression of the high affinity KdpABC transporter (**Fig. 2C)** (Laimins *et al.*, 1981).

To test these predictions, we first constructed knock-out (KO) mutants for all the K^+ transport and regulatory systems described above. We successfully inactivated all these genes except *kup*, suggesting it might be essential at least at the K^+ concentration found in the complex media PYE used to construct the KO strains. Note that a Δ*kefB* and Δ*kdpABCDE* (hereafter referred to as Δ*kdp*) were respectively used as KefBG and Kdp inactive mutants (**Fig. 2C**). Then, we measured the growth for the mutants in M2G-K supplemented with limiting (0.025 mM), abundant (0.5 mM) or

excessive (50 mM) K^+ concentrations (**Fig. 3**). In limiting K^+ conditions, only Δ*kdp* had a strong growth delay (**Fig. 3A**) whereas all the KO mutants grew as good as the WT, both in minimal and complex media supplemented with abundant K^+ concentrations (**Fig. 3B** and **Fig. S1B**). However, and as far as we know in contrast to what is described in other bacteria, a *kdp* inactive mutant could still grow in such limiting conditions, suggesting that another transporter is used in K^+-depletion conditions. At excessive K^+ concentration, we found that (i) Δ*CCNA_01688* had a slight growth delay; (ii) Δ*kdp* had a lower plateau and (iii) Δ*kefC* barely grew in comparison to WT (**Fig. 3C**). Interestingly, the growth delay of Δ*CCNA_01688* and the lower plateau of Δ*kdp* were not observed in complex PYE media supplemented with an excess of K^+ whereas Δ*kefC*, like in minimal medium, did not grow (**Fig. S1C**).

K^+-dependent essential genome

Transposon mutagenesis coupled to next-generation sequencing (Tn-seq) were used to determine a core set of genes important for adaptation and response to abundant or limiting K^+ condition. Isolated colonies harbouring transposon insertions were grown on and collected from solid agar plates. We used M2G-K with 1 % agar concentration to lower as much as possible K^+ traces from the agar in our experiment. Indeed, even at 1% agar, the K^+ traces were sufficient to allow WT cells to grow without exogenous source of K^+ (on M2G-K, **Fig. 4A**). In contrast, at least 0.025 mM K^+ had to be supplemented to M2G-K to allow growth of Δ*kdp* while at 0.5 mM K^+, both the mutant and the WT grew similarly to the growth observed on regular M2G which contains 7 mM K^+ (**Fig. 4A**). Therefore, we decided to use M2G-K without exogenous K^+ and M2G plates respectively as the limiting and abundant K^+ conditions for the Tn-seq (**Fig. 4A**).

We did calculations on the ratio of transposon (Tn) insertions per base pair (# Tn insertions / bp) for internal 80% of each ORF in each condition (M2G and M2G-K) (**Table S1**). As in studies performed in other bacteria, we analysed the frequency of Tn insertions and observed a bimodal distribution that allowed us visualizing two clusters of genes in each condition, one with low density of Tn insertions (considered as essential genes) and the other one with a higher density (considered as non-essential genes) (**Figure S2A)**. Based on this frequency of Tn insertions, we used Ward's clustering analysis (Curtis & Brun, 2014) and defined three fitness cost categories, that is (i) essential, (ii) high fitness cost (HFC) and (iii) non-essential. For the M2G library, genes with values of Tn insertions / bp ≤ 0.01333333 were considered as essential, 0.01333779 ≤ and ≤ 0.04063018 as HFC, and ≥ 0.04081632 as non-essential. For the M2G-K library, genes values of ≤ 0.0047112 were considered as essential, 0.0047909 ≤ and ≤ 0.0211178 as HFC, and ≥ 0.0215792 as non-essential (**Figure 4B** and **Table S1**). Among the 4186 annotated genes in *C. crescentus*, the percentage of essential genes in both media (M2G and M2G-K) was similar (~12 %), whilst the percentage of HFC genes was lower (~7 %) in M2G-K than in M2G (~13 %). Hence, the percentage of non-essential genes was higher in M2G-K (~ 81 %) than in M2G-K (~75 %). The shift from the HFC to the non-essential category in *C. crescentus* cells grown in M2G-K could be explained by the reduction of osmotic stress in this medium. Indeed, we showed recently that M2G generates a cell envelope stress for *C. crescentus* due to the high content of monovalent cations (Quintero-Yanes *et al.*, 2022).

Genes with known or predicted biological functions were grouped according to the classification of cluster of orthologues groups (COG) (**Fig S2B**). This allowed to highlight biological functions that are enriched in abundant and limited K^+ conditions.

Overall, the COG enrichment in the three fitness categories (Essential– E, High Fitness Cost– HFC and Non-Essential– N-E) was essentially similar in both M2G and M2G-K media. The C group “energy production and conversion” genes was the most abundant for all the fitness categories in M2G-K, as well as for E and N-E genes in M2G, while for HFC it was the second most abundant, after the J group “translation, ribosomal structure and biogenesis”.

By comparing the gene pool in each category for each media, we identified a set of 537 genes that changed their fitness cost from M2G to M2G-K and vice versa (**Fig. 4C** and **Table S2**), including 153 genes which became exclusively essential (28.5 %), 153 HFC (28.5 %) and 231 non-essential (43 %) in M2G-K. First, we observed that the TCS genes *chvGI*, known to be HFC in M2G due to its response to hyperosmotic stress (Quintero-Yanes *et al.*, 2022), became N-E in M2G-K, thereby supporting that M2G-K is a hypo-osmotic environment compared to M2G. Second, all the *kdp* genes categorised as N-E genes in M2G became essential in M2G-K except *kdpD* which became HFC. In contrast, *kup* moved from the HFC category in M2G to N-E one in M2G-K. This confirms the importance of the Kdp and Kup systems repectively in limiting and abundant K^+ conditions. Considering the conservation of the *kdp* system in bacteria, it is intriguing that *kdpD* – encoding the HK component – did not have the same fitness cost in M2G-K than the genes coding for the transporter (*kdpABC*) and the response regulator (*kdpE*) components. While this supports that KdpE likely regulates, directly, the expression of *kdpABC* genes, it suggests that KdpD and KdpE have different regulatory effects on growth in K^+-depleted environments. Finally, we did not observed changes in fitness for the other predicted potassium transport systems since all of them were categorised as N-E genes in both M2G and M2G-K,

206 further supporting that CCNA_01688, KefBG and KefC are not important for growth in
207 abundant and limiting K^+ conditions.

208

209 **Kup becomes dispensable in limiting K^+ conditions**

210 Tn-seq data suggest that inactivation of *kup* gene could be facilitated at limiting K^+
211 concentrations (**Fig. 4B**, **Tables S1** and **S2**). Kup has been described in different
212 bacteria as the major K^+ transporter, essential in hyperosmotic conditions using
213 sucrose as osmotic stressor (de Oliveira *et al.*, 2017, Trchounian & Kobayashi, 1999).
214 Moreover, in a previous study, we found that the TCS ChvGI in *C. crescentus* positively
215 controls the expression of *kup* in hyperosmotic conditions (Quintero-Yanes *et al.*,
216 2022). In agreement with this, we could not obtain a Δ*kup* strain by using a markerless,
217 SacB-dependent recombination approach on complex media (PYE) plates
218 supplemented with 3% sucrose for the counterselection. Since addition of sucrose
219 considerably increases the osmolality of the media (Hocking *et al.*, 2012), we aimed to
220 construct a Δ*kup* mutant by lowering osmolytes in the media, that is on M2G-Na-K
221 (lacking both Na_2HPO_4 and KH_2PO_4) plates supplemented with 0.5 % sucrose. In these
222 conditions, we successfully generated Δ*kup* mutant candidates that were then tested
223 for growth at different K^+ regimes. Interestingly, we observed that the Δ*kup* mutant
224 grew in limiting K^+ concentration (M2G-K supplemented with 0.025 mM K^+), although
225 at a slower growth rate but with a higher plateau compared to the WT (**Fig. 5A**). As
226 expected from the Tn-seq data, we found that Δ*kup* failed to grow when exposed to
227 abundant and excessive K^+ concentrations (**Fig. 5A**). We also confirmed that Kup is
228 essential in hypertonic conditions since the mutant did not grow in limiting K^+ conditions

when 3% sucrose were added. (**Fig. 5A**). Furthermore, we also observed that overexpression of *kup* in WT is detrimental for growth in limiting K^+ conditions (**Fig. 5B**). Altogether, these data indicate that Kup allows potassium uptake in abundant and excessive K^+ conditions but can be detrimental for unknown reasons at limiting K^+ concentrations.

While characterizing the growth of Δ*kdp* cells on M2G-K plates (**Fig. 4A**), we inadvertently selected growth suppressors. These suppressors improved the growth of Δ*kdp* in limiting K^+ conditions (**Fig. 5C**). Whole genome sequencing analyses of several of these suppressors allowed the identification of three mutations in *kup*: kup_{A87P}, kup_{G253S} and kup_{S456R}. Altogether, these data indicate that Kup allows potassium uptake in abundant and excessive K^+ conditions but unexpectedly also works at low – limiting – K^+ concentrations, and that single point mutations in Kup likely improve its affinity for K^+.

K^+- and KdpE-dependent regulons

To further characterise the response of *C. crescentus* to K^+-depleted conditions, we performed RNA-seq on RNA samples extracted from cells grown in minimal media in K^+ limiting or abundant conditions. In our experiment, we identified a total of 594 genes – 385 upregulated and 209 downregulated – whose expression was impacted upon K^+ limitation with at least a 2-fold change (FC ≥ 2) and a false-discovery rate (FDR) lower than 5% ($P_{adj} \leq 0.05$) (**Fig. 6A**). As expected, this experiment confirmed that the expression of *kdp* genes was strongly induced in the K^+-depleted medium. Among the other upregulated genes, we found genes coding for the phosphate starvation protein PhoH (CCNA_02727), a xylose isomerase family protein (CCNA_01701), a TonB-

dependent receptor (TBDR, CCNA_01859), an AraC family transcription regulator (CCNA_01858) and hypothetical proteins (CCNA_03313 and CCNA_03970) (**Fig. 6A** and **Table S3A**). Among the top downregulated candidates, we found genes expressing a small RNA (CCNA_R0158), a hemin receptor (CCNA_02277), a putative transporter (CCNA_03022), a protein with a calcium binding EF Hand binding domain (CCNA_02274) and the chaperons GroES (CCNA_00722) and GroEL (CCNA_00721) (**Fig. 6A** and **Table S3B**).

As our results suggest that the Kdp system is important for growth upon K^+ depletion, we also performed RNA-seq experiments with a Δ*kdpE* mutant grown in M2G-K supplemented with limiting K^+ concentrations. Then, we compared the RNA enrichment in Δ*kdpE vs* WT to determine which genes are affected by KdpE in a K^+-depleted condition using FC ≥ 1.5 and $P_{adj} \leq 0.05$ as parameters. Compared to WT, we found 83 upregulated and 50 downregulated genes in Δ*kdpE* grown in the K^+-depleted media (**Fig. 6B** and **Tables S4AB**). Among the 50 downregulated genes in Δ*kdpE* (**Table S4B**), 72% (36/50) were also found in the regulon of the WT starved for K^+, 19 upregulated (including *kdp* genes; **Table S3A**) and 17 downregulated (**Table S3B**). This suggests that KdpE is strictly required to activate the expression of the 19 genes in a K^+-depleted environment. On the contrary, the 17 other genes that are repressed in WT cells upon K^+ depletion are even further downregulated in the absence of KdpE, suggesting that KdpE limits the repression of these genes. The expression of the last 14 genes was insensitive to K^+ concentration while downregulated in Δ*kdpE* (**Tables S4AB**), suggesting that they are positively regulated by KdpE but independently of the K^+ concentration. Among the 83 upregulated genes in Δ*kdpE* (**Table S4A**), only ~36% (30/83) were also found in the regulon of the WT starved for K^+, 12 downregulated

(including *groEL* and *groES* genes; **Table S3B**) and 18 upregulated (**Table S3A**). This indicates KdpE is required to repress the first 12 genes upon K^+ depletion while it limits the activation of the other 18 genes in a K^+-depleted environment. The remaining 53 upregulated genes in Δ*kdpE* (**Tables S4AB**) were insensitive to K^+ availability, suggesting that they are likely repressed by KdpE but independently of the K^+ concentration.

Surprisingly, the vast majority (528 genes; 88.9 %) of the 594 genes whose expression changed in the WT grown in K^+ limiting conditions seems to be KdpE-independent, suggesting that other regulators, yet to be discovered, are activated upon K^+ depletion. An alternative explanation might be that Δ*kdpE* cells exposed to limiting K^+ concentration suffer from a general stress response, which ultimately leads to global transcriptional changes. This could also explain why half of the 163 genes (67/133) found in the Δ*kdpE* regulon were not identified in the WT regulon.

In order to unveil genes whose expression is directly regulated by KdpE, we identified the DNA regions bound by KdpE using ChIP-seq. For that, we first constructed strains in which *kdpE* was expressed under the xylose inducible promoter (P_{xylX}::*kdpE*) in a Δ*kdpE* Δ*xylX* background. Inactivating *xylX* avoids xylose consumption by *C. crescentus* as a carbon source thereby allowing constant expression of *kdpE* upon induction. Expression of *kdpE* from P_{xylX} efficiently complemented the growth of both strains in the presence of xylose since Δ*kdpE* Δ*xylX* P_{xylX}::*kdpE* cells grew similarly to the WT or Δ*xylX* cells whereas Δ*kdpDE* Δ*xylX* P_{xylX}::*kdpE* cells grew at a higher plateau (**Fig. S3A**) like Δ*kdpD* cells (see below). Moreover, using polyclonal anti-KdpE antibodies, KdpE was easily detected by western blot in both strains although KdpE protein levels were lower in Δ*kdpDE* Δ*xylX* than in Δ*kdpE* Δ*xylX* (**Fig. S3B**), suggesting

301 that KdpD has a global positive impact on KdpE levels. It is noteworthy that KdpE was
302 undetectable in WT strain, indicating that P_{xylX}::*kdpE* leads to KdpE overexpression
303 upon xylose induction.
304 A total of 110 and 146 DNA binding sites were respectively detected in the Δ*kdpE*
305 Δ*xylX* P_{xylX}::*kdpE* and Δ*kdpDE* Δ*xylX* P_{xylX}::*kdpE* strains grown in K^+ limiting conditions
306 (**Fig. 6C**; **Tables S5** and **S6**). About a third of the DNA regions bound by KdpE
307 identified in both strains – 40 out of 110 (36.4%) found in Δ*kdpE* Δ*xylX* P_{xylX}::*kdpE* and
308 46 out of 146 (31.5%) found Δ*kdpDE* Δ*xylX* P_{xylX}::*kdpE* – are located in the close vicinity
309 of genes whose expression showed a FC ≥ 1.5 in RNA-seq experiments (highlighted
310 in green in **Tables S5** and **S6**), supporting that these regions are indeed KdpE-binding
311 sites.
312 The highest numbers of reads were found in the *kdp* promoter region, not only in Δ*kdpE*
313 Δ*xylX* P_{xylX}::*kdpE* cells but more surprisingly also in Δ*kdpDE* Δ*xylX* P_{xylX}::*kdpE* cells.
314 Even more surprising is the fact that the peak for Δ*kdpDE* Δ*xylX* P_{xylX}::*kdpE* was higher
315 than in Δ*kdpE* Δ*xylX* P_{xyl}::*kdpE* (**Fig. 6C**). In fact, this is true for most of if not all the
316 regulated genes, but the difference was particularly important for the *kdp* promoter
317 (**Fig. 6D**), suggesting that KdpE could be hyperphosphorylated in the absence of KdpD
318 and therefore that KdpD mainly acts as a negative regulator of KdpE~P. Moreover, it
319 indicates that, although P_{kdp} is the main target of KdpE, multiple other genes are
320 potential direct targets of KdpE. Analysis of the top 50 sequences identified in the ChIP-
321 seq with the Δ*kdpE* Δ*xylX* P_{xylX}::*kdpE* strain using MEME allowed the identification of
322 the conserved DNA motif TCGAMRACGCSMKC likely bound by KdpE (**Fig. 6E**). For
323 the peak in the vicinity of the *kdpABCDE* operon (top hit of the analysis), the KdpE

motif was located 113 bp upstream of the *kdpA* start codon, within the gene CCNA_01662 (**Fig. 6E**).

C. crescentus KdpD regulates KdpE both positively and negatively

To further assess the role of the *C. crescentus* Kdp system in K^+-limiting conditions, we first constructed KO mutants of the transport complex (Δ*kdpABC*) and the TCS (Δ*kdpDE*) genes. In comparison to the WT, both Δ*kdpABC* and Δ*kdpDE* mutants had a growth delay at limiting but not at abundant K^+ concentration (**Fig. 7A** and **Fig. S4A**). Moreover, both mutants grew similarly, suggesting that the *kdpABC* is not expressed in the absence of the TCS, as described in other bacteria.

To study the HK *kdpD* and RR *kdpE* genes independently of each other, we constructed single KO mutants, Δ*kdpD* and Δ*kdpE*. Deletion of *kdpE* resulted in a similar growth delay than the ones displayed by Δ*kdpABC*, Δ*kdpDE* and Δ*kdpABCDE* (**Fig. 7A** and **Fig. S4B**). On the contrary, Δ*kdpD* behave differently since compared to WT, it had a slight but reproducible growth delay in exponential phase while it later reached a higher plateau in stationary phase (**Fig. 7A**). This peculiar growth behaviour was complemented by expressing *kdpD* from the native *kdp* promoter (P_{kdp}::*kdpD*) on a replicative and low-copy number plasmid in a Δ*kdpD* background (**Fig. 7B**). Complementation of the Δ*kdpE* mutant was achieved by expressing *kdpE* from the xylose inducible promoter (P_{xylX}::*kdpE*) either in a Δ*kdpE* or a Δ*kdpDE* background. While the growth defect of Δ*kdpE* was fully complemented, even in the absence of the xylose inducer, expressing back *kdpE* in Δ*kdpDE* cells led to the same growth behaviour than the single Δ*kdpD* mutant, that is a slight growth delay in exponential phase and a higher plateau in stationary phase (**Fig. 7C** and **Fig. S4C**). In addition,

348 the fact that Δ*kdpE* is epistatic on Δ*kdpD*, since Δ*kdpDE* grew as poor as Δ*kdpE* or
349 Δ*kdpABC* (**Fig. 7A**), shows KdpE is entirely responsible for the Δ*kdpD* phenotypes.
350 Together, these data support that both components of the TCS are important for WT
351 growth in K^+-depleted environments and suggest that KdpD and KdpE have
352 antagonistic roles for growth in such conditions. Kdp regulatory proteins KdpD and
353 KdpE were further analysed by identifying domains and their organisation. Comparison
354 of Pfam features highlighted that the KdpD sequence of *C. crescentus* lacks the
355 cytoplasmic GAF domain known to be linked to the DHp domain in *E. coli* [103]. Also,
356 multiple sequence alignments enabled to locate the conserved catalytic –
357 phosphorylatable – residues in both the HK (KdpD) and the RR (KdpE), that is
358 respectively the histidine 670 (His670) and the aspartate 56 (Asp56). To better
359 understand the KdpDE regulatory mechanism, we constructed *kdpD and kdpE*
360 catalytic point mutants and assessed their impact on growth in abundant and limiting
361 K^+ conditions. In agreement with what we observed with the KO mutants, all the
362 catalytic mutants grew as good as the WT in abundant K^+ conditions (**Fig. S4D**). At
363 limiting K^+ concentrations however, the phospho-ablative mutant of KdpE ($kdpE_{D56A}$)
364 had a strong growth delay, similar to the one displayed by Δ*kdpE* (**Fig. 7D** and **Fig.**
365 **S4E**). In contrast, the phospho-mimetic mutant ($kdpE_{D56E}$) grew similarly to the WT up
366 to the late exponential phase, to finally reach a higher final OD comparable to the one
367 observed with Δ*kdpD* grown in same conditions (**Fig. 7D** and **Fig. S4E**). As expected,
368 a KdpD catalytically dead mutant ($kdpD_{H670N}$) phenocopied Δ*kdpD* in limited K^+ (**Fig.**
369 **7D** and **Fig. S4E**). Since $kdpE_{D56A}$ cells had a much stronger growth delay than Δ*kdpD*
370 or $kdpD_{H670N}$, it indicates that KdpE is still phosphorylated despite the absence of KdpD
371 kinase activity. Thus, KdpE is very likely phosphorylated by another – non-cognate –

HK. On the other hand, the fact that *kdpE*$_{D56E}$ cells grew slightly but reproducibly better than Δ*kdpD* and *kdpD*$_{H670N}$ suggests that KdpD also phosphorylates KdpE, at least during the early exponential phase of growth. Thus, KdpD might (i) phosphorylate KdpE in early exponential phase, with at least another HK, and (ii) mainly act as a phosphatase on KdpE~P in late exponential phase, likely to downregulate the expression of *kdp* and restrict growth in K^+-limiting conditions.

To test this hypothesis, we constructed a KdpD kinase-deficient but phosphatase active mutant (K^-/P^+) by replacing a conserved phenylalanine residue by a leucine residue (*kdpD*$_{F832L}$) in a way reminiscent to what was described for another HK encoding gene, *pleC*$_{F778L}$ (Matroule *et al.*, 2004). Interestingly, we found that unlike the *kdpD*$_{H670N}$, *kdpD*$_{F832L}$ cells failed to reach a higher plateau in stationary phase (**Fig. 7D** and **Fig. S4E**), strongly supporting our hypothesis that KdpD primarily works as a phosphatase in late exponential phase. Moreover, the K^-/P^+ mutant *kdpD*$_{F832L}$ grew better than *kdpE*$_{D56A}$ and Δ*kdpE* mutants in low K^+ conditions (**Fig. 7D** and **Fig. S4E**), supporting that there is indeed at least another HK that phosphorylates KdpE. Finally, the fact that the *kdpD*$_{F832L}$ mutant had a growth delay compared to WT suggests that KdpD also acts as a kinase for KdpE in early exponential phase (**Fig. 7D** and **Fig. S4E**). However, we cannot rule out the possibility that the phosphatase activity of KdpD$_{F832L}$ is impacted by the mutation. For instance, it might be stronger than the WT thereby interfering with the phosphorylation levels of KdpE in early exponential phase. Nevertheless, our results altogether indicate that (i) KdpD works both as a kinase and phosphatase to control KdpE phosphorylation (KdpE~P) levels depending on the growth phase and K^+ availability and that (ii) KdpE can be phosphorylated by (an)other non-cognate HK(s) for regulating K^+ transport in K^+-depleted environments.

KdpD-dependent activation of the *kdp* promoter in low K^+ conditions

In order to study the Kdp system at the transcriptional level, a plasmid carrying a P_{kdp}::*lacZ* reporter fusion was introduced in the different mutant strains, cells were grown in limiting and abundant K^+ concentrations and β-galactosidase activity was measured. Consistent with the idea that the Kdp system is a high-affinity potassium transporter, P_{kdp} basal activity in WT cells was barely detectable (~300 Miller Units) at abundant K^+ concentration while it was strongly induced in WT (~9.000 Miller Units) or in Δ*kdpABC* cells (~10.500 Miller Units) upon K^+ depletion (**Fig. 8A**). In contrast, P_{kdp} activity was completely annihilated in Δ*kdpE* and $kdpE_{D56A}$ cells (**Fig. 8A**), indicating that phosphorylated KdpE (KdpE~P) is strictly required for *kdp* expression both in limiting and abundant K^+ conditions. In support of that, the basal activity of P_{kdp} at abundant K^+ concentration was 10 times higher (~3.000 Miller Units) in $kdpE_{D56E}$ cells than in WT cells (**Fig. 8A**). Interestingly, P_{kdp} was still active at low K^+ concentration in a Δ*kdpD,* $kdpD_{H670N}$, and $kdpD_{F832L}$ background (~4.600, ~4.200, ~4.700 Miller Units, respectively), but not to the same extent than in WT cells (~9.000 Miller Units) (**Fig. 8A**). In addition, the basal P_{kdp} activity at abundant K^+ concentration was completely abolished in the strains expressing the K^-/P^+ $kdpD_{F832L}$ variant, suggesting that the KdpD phosphatase activity is counterbalanced by its kinase activity on KdpE in K^+-replenished conditions. In support of that, compared to WT cells grown in abundat K^+ condition, the basal P_{kdp} activity was higher when both the hydrolase and kinase activities were inactivated (K^-/P^-), that is in Δ*kdpD* cells and to a lesser extent in $kdpD_{F832L}$ cells.

Then, we followed the expression of the P_{kdp}::*lacZ* fusion in WT and *kdp* mutant cells along the growth at limiting K^+ concentration. Despite Δ*kdpABC*, Δ*kdpE* and $kdpE_{D56A}$ all poorly grew in limiting K^+ conditions, P_{kdp} was active in Δ*kdpABC* cells to a level comparable to the WT one while P_{kdp} activity was almost undetectable in both *kdpE* mutants (**Fig. 8B**). These data suggest that (i) the Kdp transporter (KdpABC) is not required for *kdp* expression while (ii) the response regulator is, in contrast, indispensable. In support of this, we found the phospho-mimetic mutant of *kdpE* ($kdpE_{D56E}$) displayed a relatively constant but high activity of P_{kdp} alongside the growth curve (**Fig. 8B**).

The *kdpD* mutants had a different behaviour. First, compared to WT, the activity of P_{kdp} was Δ*kdpD* cells was lower during early exponential phase but higher in stationary phase (**Fig. 8C**). On the contrary, *kdp* expression was significantly lower both in $kdpD_{H670N}$ (K^-/P^-) and in $kdpD_{F832L}$ (K^-/P^+) during early exponential phase. However, P_{kdp} activity strongly increased only in $kdpD_{F832L}$ cells when reaching the late exponential. Altogether, these results support our hypothesis that (i) KdpD plays dual antagonistic activities on KdpE, as a kinase in early exponential phase and a phosphatase in late exponential phase of growth, and that (ii) KdpE can be phosphorylated by another non-cognate HK all along the growth.

Discussion

As the most abundant monovalent cation used by living cells to drive many cellular processes, regulating potassium (K^+) homeostasis is critical for survival. The oligotrophic α-proteobacterium *Caulobacter crescentus*, widely used as a cell cycle

model, is cyclically subjected to nutrients deprivation in its natural environments. In contrast to carbon, nitrogen or phosphate, the response of *C. crescentus* to K^+ depletion has never been characterised. Here, we first determined the range of K^+ concentrations at which *C. crescentus* supports growth. We also identified all the genes predicted to code for proteins involved the transport, the sensing and the regulation of K^+ homeostasis and tested their growth behaviour at low (limiting), optimal (abundant) and high (excessive) K^+ concentrations. Then, we defined the set of genes that (i) become essential and/or (ii) are induced upon K^+-environmental depletion. This allowed us to identify the low affinity and the high affinity K^+ transporters, respectively Kup and KdpABC, as critical components that maintain K^+ homeostasis in *C. crescentus*. Finally, we deeply characterized the role played by the two-component (TCS) regulatory system KdpDE in the response to K^+ depletion.

By analysing the Tn-Seq data, we found that the COG categories – biological functions – for which the highest number of genes became essential (EG) or high fitness cost (HFCG) upon K^+ limitation (M2G *vs* M2G-K) were (i) C "energy production and conversion" (~1% increase of EG and ~6 % increase of HFCG) and (ii) J "Translation, ribosomal structure and biogenesis" (~2% increase of EG and ~3 % increase of HFCG) (**Table S2**). In fact, it is not so surprising to highlight these two categories as sensitive to K^+ availability. Indeed, ATP concentration and respiration state are two well-known parameters that drive K^+ transport across the membrane. For instance, the electron transport chain determines the membrane potential, which in turn will influence the distribution of other ions across like K^+ that accumulate on the cytoplasmic face of the membrane. This might therefore explain why Tn-insertions in genes coding for subunits of the respiratory chain or the ATP synthase are counter-selected when K^+ become

limiting. On top of this, active transport of K^+ across the membrane by the high-affinity transporter consumes a lot of energy provided by ATP, so that decreasing ATP concentration likely has a negative impact on K^+ import. On the other hand, K^+ cations are critical for maintaining the structure and sustaining the function of ribosomes. Not only K^+ is required to stabilize the messenger RNA, the transfer RNAs, the ribosomal RNAs and the ribosomal proteins within the ribosomes, but also to increase proofreading by accommodating the right aminoacyl-tRNA in the ribosomal A-site (Grason *et al.*, 2008, Rozov *et al.*, 2019) . Additionally, many GTPases involved in translation display a K^+-dependent activation of GTP hydrolysis (Danchin & Nikel, 2019).Thus, the impact K^+ has on translation could explain the lower Tn insertion density observed in rRNA, tRNA and genes coding for ribosomal proteins in cells grown in limiting on K^+ conditions.

Several physiological processes have been described to be K^+-dependent. Besides being required by numerous enzymes related to basic metabolic functions (Danchin & Nikel, 2019, Gohara & Di Cera, 2016), such as for example the pyruvate kinase (Epstein, 2003), K^+ modulates the activity of enzymes involved in bacterial cell cycle. For instance, in *E. coli*, K^+ has been shown to stimulate the polymerisation of the cell division protein FtsZ (Ahijado-Guzman *et al.*, 2013), the activity of the DNA polymerase (Klenow & Henningsen, 1969). Moreover, the DNA supercoiling activity of the DNA gyrase was described to be triggered by K^+ in both *B. subtilis* (Gubaev & Klostermeier, 2012) and *Micrococcus luteus* (Liu & Wang, 1978). It was also described as critical for the chaperonin activity of GroEL/GroES (Grason *et al.*, 2008) or DnaK (Feifel *et al.*, 1996). Interestingly, we observed that *groEL* and *groES* became essential upon K^+

depletion, thereby suggesting that some K^+-dependent mechanisms are conserved in bacteria.

KdpDE is the major, if not the only bacterial system described in the literature to respond to limiting K^+ availability. Although KdpE was shown in *E. coli* to regulate expression of the anti-sigma factor Rsd and the ribosome modulation factor Rmf at low K^+ concentrations, thereby allowing KdpE to globally control transcription and translation in limiting K^+, other regulatory systems independent of KdpDE have not been yet described in bacteria. The K^+-dependent regulon of *C. crescentus* allowed us to identify almost 600 genes whose expression changes upon K^+ limitation. Surprisingly, only a small proportion of this regulon depends directly or indirectly on the response regulator KdpE, suggesting that there are unknown transcriptional regulators sensitive to K^+ availability.

The analysis of the *C. crescentus* genome allowed us to identify several genes and systems predicted to transport K^+. By systematically characterizing the growth profile of the corresponding mutants in different K^+ regimes, we found that the high affinity Kdp system primarily serves to import K^+ at limiting K^+ concentrations, like in many other bacterial species. Nonetheless, Kdp is unlikely the sole K^+ transport system involved in this context. Despite its growth defect, the Δ*kdpABC* mutant was still able to grow at low K^+ concentration. Since complete depletion of K^+ led to a growth arrest in *C. crescentus*, this implies that K^+ is imported by additional system(s), at least in limiting K^+ conditions. Interestingly, we found that the low affinity Kup transporter became dispensable in such limiting K^+ conditions. However, mutations in Kup have been identified to improve the growth the Δ*kdp* mutant on M2G-K plates (**Fig. 5D**), strongly suggesting that Kup participates to K^+ import when it is poorly available.

513 To test whether Kup is at work at low K^+ conditions, it might be interesting to try to
514 combine Δ*kdp* and Δ*kup* mutations together. Nonetheless, K^+ could be transported in
515 such limiting conditions by other unknown transporters. Several putative transporters
516 were identified as essential and high fitness cost in our Tn-seq analysis (i.e
517 CCNA_01159 and CCNA_00494) and up-regulated in the RNA-seq analysis (i.e
518 CCNA_00339, CCNA_01852, CCNA_01587, CCNA_01588 CCNA_02570,
519 CCNA_02571, …). It is possible that one or several of them assist the activity of
520 KdpABC in limiting K^+.

521 As in *E. coli*, the expression of *kdp* operon in *C. crescentus* is activated upon K^+
522 starvation by the KdpDE TCS (Polarek *et al.*, 1992). However, we found surprising
523 differences since in the absence of the histidine kinase (HK) KdpD, (i) *kdp* is still
524 expressed, although to a lesser extent than in WT cells and (ii) the *kdp* promoter (P_{kdp})
525 is more active in stationary phase. Our genetic dissection of the catalytic activity of
526 KdpDE with point mutants in *kdpE* (phospho-mimetic $kdpE_{D56E}$ and phospho-ablative
527 $kdpE_{D56A}$) and KdpD (K^-/P^- $kdpD_{H670N}$ and K^-/P^+ $kdpD_{F832L}$) strongly suggest that (i)
528 KdpE can be phosphorylated by another – non-cognate – HK, at least in the absence
529 of KdpD and that (ii) KdpD switches mainly to a phosphatase in late exponential phase
530 of growth.

531 In *E. coli*, deletion of the *kdpD* results in a prominent growth arrest, of more than 20
532 hours, before restarting growth thanks to KdpE phosphorylation by PhoR. However, it
533 never surpassed the WT plateau as seen with *C. crescentus* Δ*kdpD*, $kdpD_{H670N}$ and
534 $kdpE_{D56E}$ mutants. Thus, the higher plateau is due to the loss of KdpD phosphatase
535 activity. The KdpD phosphatase activity has be shown to be stimulated by intracellular
536 K^+ intracellular levels (Schramke *et al.*, 2016). Four amino acids located in the second

periplasmic loop were identified as an extracellular K^+-specific recognition site. Hence, substitution of those four amino acids by alanine resulted in a strain unable to sense extracellular K^+. In contrast, the K^+-recognition site for intracellular sensing remains to be identified. However, although specific residues could not be highlighted, the C-terminal cytoplasmic domain of KdpD was described to display a K^+-dependent phosphatase activity (Cann, 2007, Dani *et al.*, 2017). Although this has yet to be experimentally investigated, authors suggested that the cytoplasmic GAF domain of KdpD may be responsible for intracellular K^+ sensing. Most GAF domains are involved in regulatory functions through binding to cyclic nucleotides or other small ligands including ions (Cann, 2007, Heikaus *et al.*, 2009). Interestingly, we found that KdpD from *C. crescentus* lacks a GAF domain. Therefore, it is possible that such a connection between intracellular sensing and phosphatase activity does not exist in *C. crescentus*, which would explain why KdpD mainly acts as a phosphatase.

As mentioned above, in *E. coli*, the HK PhoR can crosstalk with the RR KdpE, which allows a Δ*kdpD* mutant to grow in a low K^+ environment after a long lag phase (Schramke *et al.*, 2017) . Since PhoR is conserved in *C. crescentus*, it constitutes a good candidate for the non-cognate HK phosphorylating KdpE. To test this hypothesis, we could measure growth behaviour as well as P_{kdp} activity in a strain in which both *kdpD* and *phoR* were inactivated. PhoR is a sensor kinase regulating the phosphorylation levels and activity of the RR PhoB, which drives the Pho regulon, that is the entire set of genes whose expression relies on phosphate availability. Interestingly, a crosstalk between KdpD and PhoB was also described, which means that in the absence of PhoR, PhoB can be phosphorylated by KdpD in low phosphate conditions (Schramke *et al.*, 2017) . The double crosstalk suggests there is tight

connection between K^+ and phosphate homeostasis. Since both TCS – KdpDE and PhoBR – are conserved in *C. crescentus*, it could be worth testing if the crosstalk exists in both directions as well.

Interestingly, we observed that Kup activity varies in excessive concentrations depending on the media. This indicates that Kup activity is regulated in toxic K^+ concentrations depending on environmental resources and/or metabolic states. Also, suppressor mutations that bypass the growth defect of Δ*kdp* cells in limiting K^+ conditions have been mapped in *kup* without impacting the growth when K^+ was available. A plausible explanation would be that mutations found in Kup increase its affinity for K^+, thereby increasing K^+ transport to compensate the loss of Kdp, and that the efflux systems (KefB and KefC) limits the intracellular K^+ concentration in abundant K^+ conditions. Studies in other bacteria indicate Kup is a single membrane protein showing moderate affinity for K^+ (Rhoads *et al.*, 1976, Sato *et al.*, 2014). In *Lactococcus lactis,* the second messenger c-di-AMP binds to Kup homologues, in addition to the Trk homologue, to inhibit K^+ transport (Quintana *et al.*, 2019). It is therefore possible that Kup activity is regulated by intracellular signalling molecules to coordinate K^+ uptake with environmental conditions.

KdpD homologues have also been reported to bind to c-di-AMP in other Gram-positive bacteria (Dutta *et al.*, 2021, Moscoso *et al.*, 2016). High levels of c-di-AMP inhibit the KdpD-dependent upregulation of the *kdp* operon in *Staphylococcus aureus* (Moscoso *et al.*, 2016). On top of this, genes encoding K^+ transporters are also regulated by a c-di-AMP-dependent riboswitch. The 5' leader region (LR) of the *B. subtilis kimA* transcript can adopt two mutually exclusive conformations, one favouring transcription readthrough while the other promoting transcription termination (Nelson *et al.*, 2013).

585 Upon direct binding of c-di-AMP, the *kimA* 5' LR preferentially forms a structure
586 exposing a predicted intrinsic transcription terminator, thereby inhibiting transcription
587 elongation of *kimA*. Interestingly, a study showed that transcription levels of *kimA* were
588 higher in low K^+ conditions (0.1 mM KCl) than at higher K^+ concentrations (5 mM KCl)
589 (Gundlach *et al.*, 2017). Indeed, the high-affinity K^+ transporter KimA was exclusively
590 detected in low K^+ conditions. This K^+-dependent control of *kimA* expression is
591 suggested to be achieved through a modulation of c-di-AMP intracellular levels.
592 Supporting this hypothesis, concentrations of c-di-AMP were increased by two-fold in
593 high K^+ conditions. More than just increasing in concentration, c-di-AMP becomes
594 indispensable in high K^+ conditions since a strain lacking c-di-AMP synthesising genes
595 is viable at low but not at high K^+ concentrations. *C. crescentus* produces c-di-GMP,
596 rather than c-di-AMP, to control cell development and division. If we speculate that c-
597 di-GMP levels fluctuate reminiscently to that of c-di-AMP, K^+-depletion would result in
598 low c-di-GMP levels thereby preventing progression in cell cycle. Although it remains
599 unclear how K^+ limitation leads to a decrease in c-di-AMP levels, it has been shown
600 that the enzymes producing c-di-AMP in *B. subtilis* were less abundant in low K^+
601 conditions (Gundlach *et al.*, 2017). Evaluating the growth behaviour of cells unable to
602 synthesize c-di-GMP (Abel *et al.*, 2013) in excessive or limiting K^+ conditions could be
603 an initial step to assess if such regulation is conserved.

604 The nitrogen-related phosphotransferase component $EIIA^{Ntr}$ has been shown in *E. coli*
605 to regulate not only K^+ transport, by modulating KdpD kinase activity (Luttmann *et al.*,
606 2015, Mork-Morkenstein *et al.*, 2017, Zimmer *et al.*, 2008) but also phosphate
607 starvation response, by modulating PhoR activity (Luttmann *et al.*, 2012). For instance,
608 in limiting K^+ conditions (< 5 mM), the unphosphorylated form of $EIIA^{Ntr}$ was shown to

directly interact with KdpD and stimulate its kinase activity, thereby promoting phosphorylation of KdpE and the subsequent increase of *kdp* genes expression (Luttmann *et al.*, 2009). This $EIIA^{Ntr}$-based control of KdpD has also been reported in the plant symbionts *Rhizobium leguminosarum* (Untiet *et al.*, 2013) and *Sinorhizobium fredii* (Feng *et al.*, 2022), two α-proteobacteria closely related to *C. crescentus*. It was later discovered that $EIIA^{Ntr}$ regulates in fact sigma factor selectivity by modulating K^+ levels. Indeed, the competition between σ^{70} and σ^S for interaction with the RNA polymerase (RNAP) is influenced by K^+ intracellular levels (Lee *et al.*, 2010). Depending on the phosphorylation state of $EIIA^{Ntr}$, the resulting K^+ intracellular levels preferentially favour the binding of either σ^{70} or σ^S to the core RNAP (Lee *et al.*, 2010). Interestingly, PTS^{Ntr} components regulate the levels of another signalling molecule – (p)ppGpp – that connects cell division with environmental and metabolic cues in *C. crescentus* (Hallez *et al.*, 2017, Ronneau *et al.*, 2016, Shyp *et al.*, 2021). Knowing that (p)ppGpp also influences gene expression by regulating sigma factor competition (Jishage *et al.*, 2002), it is therefore tempting to speculate that $EIIA^{Ntr}$ and/or (p)ppGpp participate to the K^+ homeostasis in *C. crescentus*, even in other alphaproteobacteria.

We also generated strains in which either *kefB* or *kefC* – both coding for efflux pumps – was inactivated. We observed that deletion of *kefC* (Δ*kefC*) dramatically impaired growth in excess of K^+, while the *kefB* mutant (Δ*kefB*) behaved like the WT strain, suggesting that KefB cannot support KefC functions. Recently, it was reported that glutathione controls cell division via negative regulation of the potassium (K^+) efflux pump KefB (Hartl *et al.*, 2020). Indeed, cell filamentation and decreased intracellular K^+ levels were observed in mutants unable to synthesize glutathione (Δ*gshB*), suggesting that K^+ homeostasis is crucial for bacterial cell cycle regulation.

Interestingly, mutations that suppressed Δ*gshB* phenotypes were found in *kefB* and *kefG*, but not in *kefC*. This indicated that, glutathione regulation in *C. crescentus* occurs mainly through *kefB*. Therefore, it is likely that the glutathione-dependent negative regulation on KefB still occurred in Δ*kefC* cells, which would explain why the single *kefC* knock-out mutant failed to grow when K^+ was in excess whereas the single Δ*kefC* grew.

Methods

Bacterial strains and growth conditions.

All *Escherichia coli* strains used in this thesis were grown aerobically in Luria-Bertani (LB) broth (Sigma). *E. coli* Top10 was used for cloning purpose while *E. coli* MT607 was used for triparental matings. Thermo-competent cells were used for transformation of *E. coli.* All *Caulobacter crescentus* strains used are derived from the synchronizable wild-type strain NA1000. The traditional synthetic media supplemented with glucose (M2G) was modified by replacing potassium salts by their equivalent sodium salts to obtain a medium without any K^+ (K_0) to which the desired K^+ concentrations could be added. The source of K^+ consists in both KH_2PO_4 and K_2HPO_4 mixed to an equivalent ratio in terms of K^+ concentration. For each experiment, cells were first grown at 30 °C; in Peptone Yeast Extract (PYE), then adapted overnight at 30 °C in K_0 media supplemented with 0.5 mM K^+, washed twice in K_0 media and finally grown at 30 °C in K_0 media supplemented with the desired K^+ concentration. For growth curve measurements, cultures were diluted to a final OD_{660} of 0.02 in a 96-well plate. Growth was monitored during 48 h with continuous shaking at 30 °C, in an automated plate

reader (Bioscreen C, Lab Systems) measuring OD_{660} every 10 min. For *E. coli*, antibiotics were used at the following concentrations (μg/ml; in liquid/solid medium): chloramphenicol (20/30), kanamycin (30/50), oxytetracycline (12.5/12.5), spectinomycin (100/100), streptomycin (50/100) while for *C. crescentus*, media were supplemented with kanamycin (5/20), oxytetracycline (2.5/2.5), nalidixic acid (20) when appropriate. Genes under the control of the inducible xylose promoter (P_{xylX}) were induced with 0.1 % xylose. Plasmid delivery into *C. crescentus* was achieved by either bi- or tri-parental mating using *E. coli* S17-1 and *E. coli* MT607 as helper strains, respectively. In-frame deletions were created by using the pNPTS138-derivative plasmids as follows. Integration of the plasmids in the *C. crescentus* genome after single homologous recombination were selected on PYE plates supplemented with kanamycin. Three independent recombinant clones were inoculated in PYE medium without kanamycin and incubated overnight at 30 °C. Then, dilutions were spread on PYE plates supplemented with 3% sucrose and incubated at 30 °C. Single colonies were picked and transferred onto PYE plates with and without kanamycin. Finally, to discriminate between mutated and wild-type loci, kanamycin-sensitive clones were tested by PCR on colony using locus-specific oligonucleotides.

Spotting assays

Ten-fold serial dilutions (in M2G-K) were prepared in 96-well plates from 5 ml cultures in standard universal tubes grown overnight at 30 °C in the corresponding media. Cells (5μl) were then spotted on plates, incubated at 30 °C for two-to-three days and pictures were taken.

β-galactosidase assays

β-galactosidase assays were performed as already described in (Quintero-Yanes *et al.*, 2022). Briefly, cultures were either grown to stationary phase directly in a 96-wells plate or grown in flasks from which samples were withdrawn throughout growth and placed at -80 °C in between time points. Permeabilization of cells was performed by incubating cells with lysis buffer (20 mg/ml polymyxin B, β-mercaptoethanol) for 30 min at 28 °C. Then, 50 µl of 4 mg/ml O-nitrophenyl- β-D-galactopyranoside (ONPG) were added. Lysis and ONPG solutions were prepared using Z buffer as a solvent (60 mM Na_2HPO_4, 40 mM NaH_2PO_4, 10 mM KCl, 1 mM $MgSO_4$, pH 7.0). Both OD_{420} and OD_{550} were measured every minute for 30 min at 30 °C using a fluorimeter (SpectraMax®, Molecular Devices). Miller Units were calculated using the following formula: M.U. = $\frac{[OD420 - (1.75\ x\ OD550)]x\ 1000}{OD660x\ t\ x\ v}$ where t is the reaction time in min v is the volume of culture used in ml. Then, ONPG hydrolysis was measured at 30 °C for 30 min. The activity of the β-galactosidase expressed in miller units (MU) was calculated using the following equation: MU = (OD_{420} × 1,000) / [OD_{660} × t × v] where "t" is the time of the reaction (min), and "v" is the volume of cultures used in the assays (ml). Experimental values were the average of three independent experiments.

Protein purification and production of polyclonal antibodies

To immunize rabbits for production of polyclonal antibodies, an *E. coli* BL21 (DE3) pLysS strain carrying plasmid pET-28a-*kdpE* was grown in LB medium supplemented with kanamycin and chloramphenicol until an OD600 of 0.5. After addition of IPTG to a final concentration of 1 mM, the culture was incubated at 18 °C for 18 hrs. Cells were then harvested by centrifugation for 30 min at 5,000 x g, 4 °C. The pellet was resuspended in 20 ml of binding buffer (20 mM Tris-HCl pH 8.0, 500 mM NaCl, 10% glycerol, 10 mM $MgCl_2$, 12.5 mM Imidazole) supplemented with complete EDTA-free

protease cocktail inhibitor (Roche), 400 mg lysozyme (Sigma) and 10 mg DNaseI (Roche) and incubated for 30 min on ice. Cells were then lysed by sonication. After centrifugation at 12,000 rpm for 30 min at 4°C, the lysate was loaded on a Ni-NTA column and incubated 1 hr at 4 °C with end-over-end agitation. The column was then washed with 5 ml binding buffer, 3 ml Wash1 buffer (binding buffer with 25 mM imidazole), 3 ml Wash2 buffer (binding buffer with 50 mM imidazole), 3 ml Wash3 buffer (binding buffer with 75 mM imidazole). Proteins bound to the column were eluted with 3 ml Elution buffer (binding buffer with 100 mM imidazole) and aliquoted in 300 μl fractions. All the fractions containing the protein of interest (checked by Coomassie blue staining) were pooled and dialyzed in Dialysis buffer (20 mM Tris pH 8, 500 mM NaCl, 10% glycerol). Purified KdpE was used to immunize rabbits (CER Groupe, Marloie, Belgium).

Tn-seq analysis.

A mini-Tn5 was introduced in *C. crescentus* NA1000 WT strain by bi-parental mating. Briefly, overnight cultures of recipient and donor strains (grown in LB supplemented with kanamycin) were mixed in 95:5 ratio to a final volume of 1 ml. Cells were harvested by centrifugation at 9,000 rpm (7,600 x g) at room temperature for 2 min. The supernatant was removed, and 1 ml of fresh PYE medium was added to wash the pellet. A second centrifugation step was done to remove again the supernatant. Thereafter, the pellet was resuspended in 50 μl and spotted on PYE agar and incubated at 30 ° C for 4h. Cells were collected, resuspended in 10 ml M2G or M2G-K and washed twice with the same volume. Dilutions (10^{-6}) were plated on M2G or M2G-K plates supplemented with aztreonam (5μg l^{-1}) and kanamycin (5μg l^{-1}) and incubated at 30 ° C for 5 days. Then, at least 3 x10^5 colonies were collected in M2G or M2G-K

supplemented with 10% glycerol and stored at -80 °C. Genomic DNA was then extracted following the *Nucleospin Tissue Kit* protocol (Macherey-Nagel) and resuspended in 50 µl elution buffer (5 mM Tris-HCl [pH 8.5]). DNA sequencing was performed using an Illumina NextSeq (paired-end 2x75) instrument (Fasteris, Geneva, Switzerland). Reads corresponding to the mini-Tn5 insertion sites were first filtered with the 5'-GGTTGAGATGTGTATAAGAGACAG sequence before being processed as described in (Coppine *et al.*, 2020). Briefly, filtered reads were mapped on the genome of *C. crescentus* NA1000 (GenBank accession number NC_011916.1) and converted to Sequence Alignment/Map (SAM) format using the Burrows-Wheeler Aligner (BWA) and SAMtools, respectively, from the Sourceforge server (https://sourceforge.net/). Next, the number of reads overlapping each genomic position was computed using custom Python scripts. The total number of reads for internal 80% of each ORF in each condition were then computed using custom Python scripts. For comparing strains, the total number of reads was normalized by the ratio of the number of reads between the two strains. Ward's clustering analysis was performed to define the fitness categories as previously reported.

Chromatin immunoprecipitation followed by deep sequencing (ChIP-Seq assay)

ChIP-Seq was performed as already described in (Coppine *et al.*, 2020). Briefly, 80 ml of mid-log-phase cells (OD_{660} of 0.6) were cross-linked in 1% formaldehyde and 10 mM sodium phosphate (pH 7.6) at room temperature (RT) for 10 min and then for 30 min on ice. Cross-linking was stopped by addition of 125 mM glycine and incubated for 5 min on ice. Cells were washed twice in phosphate buffer solution (PBS; 137 mM NaCl, 2.7 mM KCl, 10 mM Na_2HPO_4, 1.8 mM KH_2PO_4, pH 7.4) resuspended in 450 µl TES buffer (10 mM Tris-HCl [pH 7.5], 1 mM EDTA, and 100 mM NaCl), and lysed with

2 μl of Ready-lyse lysozyme solution for 5 min at RT. Protease inhibitors (Roche) were added, and the mixture was incubated for 10 min. Then, 550 μl of ChIP buffer (1.1% Triton X-100, 1.2 mM EDTA, 16.7 mM Tris-HCl [pH 8.1], 167 mM NaCl, protease inhibitors) were added to the lysate and incubated at 37 °C for 10 min before sonication (2 x 8 bursts of 30 sec on ice using a Diagenode Bioruptor) to shear DNA fragments to a length of 300 to 500 bp. Lysate was cleared by centrifugation for 10 min at 12,500 rpm at 4 °C, and protein content was assessed by measuring the OD_{280}. Then, 7.5 mg of proteins was diluted in ChIP buffer supplemented with 0.01% SDS and precleared for 1 hr at 4 °C with 50 μl of SureBeads Protein A Magnetic Beads (BioRad) and 100 μg bovine serum albumin (BSA). One microliter of polyclonal anti-KdpE antibodies was added to the supernatant before overnight incubation at 4 °C under gentle agitation. Next, 80 μl of BSA presaturated protein A-agarose beads were added to the solution and incubated for 2 hrs at 4 °C with rotation, washed once with low-salt buffer (0.1% SDS, 1% Triton X-100, 2 mM EDTA, 20 mM Tris-HCl [pH 8.1], 150 mM NaCl), once with high-salt buffer (0.1% SDS, 1% Triton X-100, 2 mM EDTA, 20 mM Tris-HCl [pH 8.1], 500 mM NaCl), once with LiCl buffer (0.25 M LiCl, 1% NP-40, 1% deoxycholate, 1 mM EDTA, 10 mM Tris-HCl [pH 8.1]), and once with TE buffer (10 mM Tris-HCl [pH 8.1] 1 mM EDTA) at 4 °C, followed by a second wash with TE buffer at RT. The DNA-protein complexes were eluted twice in 250 μl freshly prepared elution buffer (0.1 M NaHCO3, 1% SDS). NaCl was added at a concentration of 300 mM to the combined eluates (500 μl) before overnight incubation at 65 °C to reverse the cross-link. The samples were treated with 20 μg of proteinase K in 40mM EDTA and 40 mM Tris-HCl (pH 6.5) for 2 h at 45 °C. DNA was extracted using a Nucleospin PCR cleanup kit (Macherey-Nagel) and resuspended in 50 μl elution buffer (5 mM Tris-HCl [pH 8.5]).

DNA sequencing was performed using an Illumina NextSeq 550 (paired-end 2x75) instrument (Seqalis). NGS data were analysed as described in (Coppine *et al.*, 2020).

RNA-Seq

WT and Δ*kdpE* cells were grown overnight to OD_{660} ~ 0.3 in M2G-K 0,025 mM K^+ and WT in M2G-K 0,5 mM K^+. Thereafter, total RNA was extracted with RNeasy® Protect Bacteria Kit from Qiagen and following manufacturer's instructions. The quantity and quality (A260/A280 ration) of RNA was determined with a Thermo Scientific™ Nanodrop ™ One Microvolume UV-Vis Spectrophotometer. RNA-Seq TTRNA libraries were prepared according to the manufacturer's instructions and sequenced with Illumina NovaSeq 6000 (paired-end 2x100) instrument (Seqalis). NGS data were analysed using Galaxy (https://usegalaxy.org) (Quintero-Yanes *et al.*, 2022). Briefly, FastQC was used to evaluate the quality of the reads; HISAT2 was used to map the reads onto the NA1000 reference genome (NC_011916.1) and generate bam files; featureCounts was used to generate counts tables using bam files and DESeq2 was used to determine differentially expressed genes. The Volcano plot was generated using GraphPad Prism 9 software.

MEME analysis

Sequences corresponding to the peaks founds in ChIP-seq were analysed for a KdpE conserved DNA binding motif using MEME (Quintero-Yanes *et al.*, 2022) (**Table S6**). As searching parameters, the classical motif discovery mode, zoops motif site distribution, 10 minimum motif width and 20 maximum motif width, 2 as maximum number of motifs and a p-value<0.001 as cut-off were used. The motif with highest site count was selected.

Statistical analyses

All the statistical analyses were performed using GraphPad Prism 9 software. A *P* value of <0.05 was considered as significant.

Data availability

ChIP-Seq and RNA-Seq data have been deposited to the Gene Expression Omnibus (GEO) repository with the accession number XXX.

References

Abel, S., Bucher, T., Nicollier, M., Hug, I., Kaever, V., Abel Zur Wiesch, P., and Jenal, U. (2013) Bi-modal distribution of the second messenger c-di-GMP controls cell fate and asymmetry during the caulobacter cell cycle. *PLoS Genet* **9**: e1003744.

Ahijado-Guzman, R., Alfonso, C., Reija, B., Salvarelli, E., Mingorance, J., Zorrilla, S., Monterroso, B., and Rivas, G. (2013) Control by potassium of the size distribution of Escherichia coli FtsZ polymers is independent of GTPase activity. *J Biol Chem* **288**: 27358-27365.

Ali, M.K., Li, X., Tang, Q., Liu, X., Chen, F., Xiao, J., Ali, M., Chou, S.H., and He, J. (2017) Regulation of Inducible Potassium Transporter KdpFABC by the KdpD/KdpE Two-Component System in Mycobacterium smegmatis. *Front Microbiol* **8**: 570.

Bakker, E.P., and Mangerich, W.E. (1981) Interconversion of components of the bacterial proton motive force by electrogenic potassium transport. *J Bacteriol* **147**: 820-826.

Booth, I.R. (1999) The regulation of intracellular pH in bacteria. *Novartis Found Symp* **221**: 19-28; discussions 28-37.

Bossemeyer, D., Borchard, A., Dosch, D.C., Helmer, G.C., Epstein, W., Booth, I.R., and Bakker, E.P. (1989a) K+-transport protein TrkA of Escherichia coli is a peripheral membrane protein that requires other trk gene products for attachment to the cytoplasmic membrane. *J Biol Chem* **264**: 16403-16410.

Bossemeyer, D., Schlosser, A., and Bakker, E.P. (1989b) Specific cesium transport via the Escherichia coli Kup (TrkD) K+ uptake system. *J Bacteriol* **171**: 2219-2221.

Cann, M. (2007) A subset of GAF domains are evolutionarily conserved sodium sensors. *Mol Microbiol* **64**: 461-472.

Cao, Y., Jin, X., Huang, H., Derebe, M.G., Levin, E.J., Kabaleeswaran, V., Pan, Y., Punta, M., Love, J., Weng, J., Quick, M., Ye, S., Kloss, B., Bruni, R., Martinez-Hackert, E., Hendrickson, W.A., Rost, B., Javitch, J.A., Rajashankar, K.R., Jiang, Y., and Zhou, M. (2011) Crystal structure of a potassium ion transporter, TrkH. *Nature* **471**: 336-340.

Castaneda-Garcia, A., Do, T.T., and Blazquez, J. (2011) The K+ uptake regulator TrkA controls membrane potential, pH homeostasis and multidrug susceptibility in Mycobacterium smegmatis. *J Antimicrob Chemother* **66**: 1489-1498.

Coppine, J., Kaczmarczyk, A., Petit, K., Brochier, T., Jenal, U., and Hallez, R. (2020) Regulation of Bacterial Cell Cycle Progression by Redundant Phosphatases. *J Bacteriol* **202**.

Curtis, P.D., and Brun, Y.V. (2014) Identification of essential alphaproteobacterial genes reveals operational variability in conserved developmental and cell cycle systems. *Mol Microbiol* **93**: 713-735.
Danchin, A., and Nikel, P.I. (2019) Why Nature Chose Potassium. *J Mol Evol* **87**: 271-288.
Dani, P., Ujaoney, A.K., Apte, S.K., and Basu, B. (2017) Regulation of potassium dependent ATPase (kdp) operon of Deinococcus radiodurans. *PLoS One* **12**: e0188998.
de Oliveira, M.V., Intorne, A.C., Vespoli, L.S., Andrade, L.F., Pereira, L.M., Rangel, P.L., and de Souza Filho, G.A. (2017) Essential role of K(+) uptake permease (Kup) for resistance to sucrose-induced stress in Gluconacetobacter diazotrophicus PAl 5. *Environ Microbiol Rep* **9**: 85-90.
Dominguez-Ferreras, A., Munoz, S., Olivares, J., Soto, M.J., and Sanjuan, J. (2009) Role of potassium uptake systems in Sinorhizobium meliloti osmoadaptation and symbiotic performance. *J Bacteriol* **191**: 2133-2143.
Dosch, D.C., Helmer, G.L., Sutton, S.H., Salvacion, F.F., and Epstein, W. (1991) Genetic analysis of potassium transport loci in Escherichia coli: evidence for three constitutive systems mediating uptake potassium. *J Bacteriol* **173**: 687-696.
Dutta, A., Batish, M., and Parashar, V. (2021) Structural basis of KdpD histidine kinase binding to the second messenger c-di-AMP. *J Biol Chem* **296**: 100771.
Epstein, W. (2003) The roles and regulation of potassium in bacteria. *Prog Nucleic Acid Res Mol Biol* **75**: 293-320.
Feifel, B., Sandmeier, E., Schonfeld, H.J., and Christen, P. (1996) Potassium ions and the molecular-chaperone activity of DnaK. *Eur J Biochem* **237**: 318-321.
Feng, X.Y., Tian, Y., Cui, W.J., Li, Y.Z., Wang, D., Liu, Y., Jiao, J., Chen, W.X., and Tian, C.F. (2022) The PTS(Ntr)-KdpDE-KdpFABC Pathway Contributes to Low Potassium Stress Adaptation and Competitive Nodulation of Sinorhizobium fredii. *mBio* **13**: e0372121.
Gohara, D.W., and Di Cera, E. (2016) Molecular Mechanisms of Enzyme Activation by Monovalent Cations. *J Biol Chem* **291**: 20840-20848.
Grason, J.P., Gresham, J.S., Widjaja, L., Wehri, S.C., and Lorimer, G.H. (2008) Setting the chaperonin timer: the effects of K+ and substrate protein on ATP hydrolysis. *Proc Natl Acad Sci U S A* **105**: 17334-17338.
Gries, C.M., Bose, J.L., Nuxoll, A.S., Fey, P.D., and Bayles, K.W. (2013) The Ktr potassium transport system in Staphylococcus aureus and its role in cell physiology, antimicrobial resistance and pathogenesis. *Mol Microbiol* **89**: 760-773.
Gubaev, A., and Klostermeier, D. (2012) Potassium ions are required for nucleotide-induced closure of gyrase N-gate. *J Biol Chem* **287**: 10916-10921.
Gundlach, J., Herzberg, C., Kaever, V., Gunka, K., Hoffmann, T., Weiss, M., Gibhardt, J., Thurmer, A., Hertel, D., Daniel, R., Bremer, E., Commichau, F.M., and Stulke, J. (2017) Control of potassium homeostasis is an essential function of the second messenger cyclic di-AMP in Bacillus subtilis. *Sci Signal* **10**.
Hallez, R., Delaby, M., Sanselicio, S., and Viollier, P.H. (2017) Hit the right spots: cell cycle control by phosphorylated guanosines in alphaproteobacteria. *Nat Rev Microbiol* **15**: 137-148.
Harms, C., Domoto, Y., Celik, C., Rahe, E., Stumpe, S., Schmid, R., Nakamura, T., and Bakker, E.P. (2001) Identification of the ABC protein SapD as the subunit that confers ATP dependence to the K+-uptake systems Trk(H) and Trk(G) from Escherichia coli K-12. *Microbiology (Reading)* **147**: 2991-3003.

881 Hartl, J., Kiefer, P., Kaczmarczyk, A., Mittelviefhaus, M., Meyer, F., Vonderach, T., Hattendorf,
882 B., Jenal, U., and Vorholt, J.A. (2020) Untargeted metabolomics links glutathione to
883 bacterial cell cycle progression. *Nat Metab* **2**: 153-166.
884 Heermann, R., and Jung, K. (2010) The complexity of the 'simple' two-component system
885 KdpD/KdpE in Escherichia coli. *FEMS Microbiol Lett* **304**: 97-106.
886 Heikaus, C.C., Pandit, J., and Klevit, R.E. (2009) Cyclic nucleotide binding GAF domains from
887 phosphodiesterases: structural and mechanistic insights. *Structure* **17**: 1551-1557.
888 Hocking, J., Priyadarshini, R., Takacs, C.N., Costa, T., Dye, N.A., Shapiro, L., Vollmer, W., and
889 Jacobs-Wagner, C. (2012) Osmolality-dependent relocation of penicillin-binding
890 protein PBP2 to the division site in Caulobacter crescentus. *J Bacteriol* **194**: 3116-3127.
891 Humphries, J., Xiong, L., Liu, J., Prindle, A., Yuan, F., Arjes, H.A., Tsimring, L., and Suel, G.M.
892 (2017) Species-Independent Attraction to Biofilms through Electrical Signaling. *Cell*
893 **168**: 200-209 e212.
894 Jishage, M., Kvint, K., Shingler, V., and Nystrom, T. (2002) Regulation of sigma factor
895 competition by the alarmone ppGpp. *Genes Dev* **16**: 1260-1270.
896 Karp, P.D., Billington, R., Caspi, R., Fulcher, C.A., Latendresse, M., Kothari, A., Keseler, I.M.,
897 Krummenacker, M., Midford, P.E., Ong, Q., Ong, W.K., Paley, S.M., and Subhraveti, P.
898 (2019) The BioCyc collection of microbial genomes and metabolic pathways. *Brief*
899 *Bioinform* **20**: 1085-1093.
900 Klenow, H., and Henningsen, I. (1969) Effect of monovalent cations on the activity of the DNA
901 polymerase of Escherichia coli B. *Eur J Biochem* **9**: 133-141.
902 Laimins, L.A., Rhoads, D.B., and Epstein, W. (1981) Osmotic control of kdp operon expression
903 in Escherichia coli. *Proc Natl Acad Sci U S A* **78**: 464-468.
904 Lee, C.R., Cho, S.H., Kim, H.J., Kim, M., Peterkofsky, A., and Seok, Y.J. (2010) Potassium
905 mediates Escherichia coli enzyme IIA(Ntr) -dependent regulation of sigma factor
906 selectivity. *Mol Microbiol* **78**: 1468-1483.
907 Liu, L.F., and Wang, J.C. (1978) Micrococcus luteus DNA gyrase: active components and a
908 model for its supercoiling of DNA. *Proc Natl Acad Sci U S A* **75**: 2098-2102.
909 Liu, Y., Ho, K.K., Su, J., Gong, H., Chang, A.C., and Lu, S. (2013) Potassium transport of
910 Salmonella is important for type III secretion and pathogenesis. *Microbiology*
911 *(Reading)* **159**: 1705-1719.
912 Luttmann, D., Gopel, Y., and Gorke, B. (2012) The phosphotransferase protein EIIA(Ntr)
913 modulates the phosphate starvation response through interaction with histidine
914 kinase PhoR in Escherichia coli. *Mol Microbiol* **86**: 96-110.
915 Luttmann, D., Gopel, Y., and Gorke, B. (2015) Cross-Talk between the Canonical and the
916 Nitrogen-Related Phosphotransferase Systems Modulates Synthesis of the KdpFABC
917 Potassium Transporter in Escherichia coli. *J Mol Microbiol Biotechnol* **25**: 168-177.
918 Luttmann, D., Heermann, R., Zimmer, B., Hillmann, A., Rampp, I.S., Jung, K., and Gorke, B.
919 (2009) Stimulation of the potassium sensor KdpD kinase activity by interaction with
920 the phosphotransferase protein IIA(Ntr) in Escherichia coli. *Mol Microbiol* **72**: 978-994.
921 MacGilvary, N.J., Kevorkian, Y.L., and Tan, S. (2019) Potassium response and homeostasis in
922 Mycobacterium tuberculosis modulates environmental adaptation and is important
923 for host colonization. *PLoS Pathog* **15**: e1007591.
924 Matroule, J.Y., Lam, H., Burnette, D.T., and Jacobs-Wagner, C. (2004) Cytokinesis monitoring
925 during development; rapid pole-to-pole shuttling of a signaling protein by localized
926 kinase and phosphatase in Caulobacter. *Cell* **118**: 579-590.

927 Mork-Morkenstein, M., Heermann, R., Gopel, Y., Jung, K., and Gorke, B. (2017) Non-canonical
928 activation of histidine kinase KdpD by phosphotransferase protein PtsN through
929 interaction with the transmitter domain. *Mol Microbiol* **106**: 54-73.
930 Moscoso, J.A., Schramke, H., Zhang, Y., Tosi, T., Dehbi, A., Jung, K., and Grundling, A. (2016)
931 Binding of Cyclic Di-AMP to the Staphylococcus aureus Sensor Kinase KdpD Occurs via
932 the Universal Stress Protein Domain and Downregulates the Expression of the Kdp
933 Potassium Transporter. *J Bacteriol* **198**: 98-110.
934 Nelson, J.W., Sudarsan, N., Furukawa, K., Weinberg, Z., Wang, J.X., and Breaker, R.R. (2013)
935 Riboswitches in eubacteria sense the second messenger c-di-AMP. *Nat Chem Biol* **9**:
936 834-839.
937 Ochrombel, I., Ott, L., Kramer, R., Burkovski, A., and Marin, K. (2011) Impact of improved
938 potassium accumulation on pH homeostasis, membrane potential adjustment and
939 survival of Corynebacterium glutamicum. *Biochim Biophys Acta* **1807**: 444-450.
940 Pedersen, B.P., Stokes, D.L., and Apell, H.J. (2019) The KdpFABC complex - K(+) transport
941 against all odds. *Mol Membr Biol* **35**: 21-38.
942 Polarek, J.W., Williams, G., and Epstein, W. (1992) The products of the kdpDE operon are
943 required for expression of the Kdp ATPase of Escherichia coli. *J Bacteriol* **174**: 2145-
944 2151.
945 Prindle, A., Liu, J., Asally, M., Ly, S., Garcia-Ojalvo, J., and Suel, G.M. (2015) Ion channels enable
946 electrical communication in bacterial communities. *Nature* **527**: 59-63.
947 Quintana, I.M., Gibhardt, J., Turdiev, A., Hammer, E., Commichau, F.M., Lee, V.T., Magni, C.,
948 and Stulke, J. (2019) The KupA and KupB Proteins of Lactococcus lactis IL1403 Are
949 Novel c-di-AMP Receptor Proteins Responsible for Potassium Uptake. *J Bacteriol* **201**.
950 Quintero-Yanes, A., Mayard, A., and Hallez, R. (2022) The two-component system ChvGI
951 maintains cell envelope homeostasis in Caulobacter crescentus. *PLoS Genet* **18**:
952 e1010465.
953 Quintero-Yanes, A., Monson, R.E., and Salmond, G.P.C. (2019) Environmental potassium
954 regulates bacterial flotation, antibiotic production and turgor pressure in Serratia
955 through the TrkH transporter. *Environ Microbiol* **21**: 2499-2510.
956 Rasmussen, T. (2023) The Potassium Efflux System Kef: Bacterial Protection against Toxic
957 Electrophilic Compounds. *Membranes (Basel)* **13**.
958 Rhoads, D.B., Waters, F.B., and Epstein, W. (1976) Cation transport in Escherichia coli. VIII.
959 Potassium transport mutants. *J Gen Physiol* **67**: 325-341.
960 Roe, A.J., McLaggan, D., O'Byrne, C.P., and Booth, I.R. (2000) Rapid inactivation of the
961 Escherichia coli Kdp K+ uptake system by high potassium concentrations. *Mol*
962 *Microbiol* **35**: 1235-1243.
963 Ronneau, S., Petit, K., De Bolle, X., and Hallez, R. (2016) Phosphotransferase-dependent
964 accumulation of (p)ppGpp in response to glutamine deprivation in Caulobacter
965 crescentus. *Nat Commun* **7**: 11423.
966 Roosild, T.P., Castronovo, S., Healy, J., Miller, S., Pliotas, C., Rasmussen, T., Bartlett, W.,
967 Conway, S.J., and Booth, I.R. (2010) Mechanism of ligand-gated potassium efflux in
968 bacterial pathogens. *Proc Natl Acad Sci U S A* **107**: 19784-19789.
969 Rozov, A., Khusainov, I., El Omari, K., Duman, R., Mykhaylyk, V., Yusupov, M., Westhof, E.,
970 Wagner, A., and Yusupova, G. (2019) Importance of potassium ions for ribosome
971 structure and function revealed by long-wavelength X-ray diffraction. *Nat Commun* **10**:
972 2519.

Sato, Y., Nanatani, K., Hamamoto, S., Shimizu, M., Takahashi, M., Tabuchi-Kobayashi, M., Mizutani, A., Schroeder, J.I., Souma, S., and Uozumi, N. (2014) Defining membrane spanning domains and crucial membrane-localized acidic amino acid residues for K(+) transport of a Kup/HAK/KT-type Escherichia coli potassium transporter. *J Biochem* **155**: 315-323.

Schleyer, M., and Bakker, E.P. (1993) Nucleotide sequence and 3'-end deletion studies indicate that the K(+)-uptake protein kup from Escherichia coli is composed of a hydrophobic core linked to a large and partially essential hydrophilic C terminus. *J Bacteriol* **175**: 6925-6931.

Schramke, H., Laermann, V., Tegetmeyer, H.E., Brachmann, A., Jung, K., and Altendorf, K. (2017) Revisiting regulation of potassium homeostasis in Escherichia coli: the connection to phosphate limitation. *Microbiologyopen* **6**.

Schramke, H., Tostevin, F., Heermann, R., Gerland, U., and Jung, K. (2016) A Dual-Sensing Receptor Confers Robust Cellular Homeostasis. *Cell Rep* **16**: 213-221.

Shyp, V., Dubey, B.N., Bohm, R., Hartl, J., Nesper, J., Vorholt, J.A., Hiller, S., Schirmer, T., and Jenal, U. (2021) Reciprocal growth control by competitive binding of nucleotide second messengers to a metabolic switch in Caulobacter crescentus. *Nat Microbiol* **6**: 59-72.

Su, J., Gong, H., Lai, J., Main, A., and Lu, S. (2009) The potassium transporter Trk and external potassium modulate Salmonella enterica protein secretion and virulence. *Infect Immun* **77**: 667-675.

Trchounian, A., and Kobayashi, H. (1999) Kup is the major K+ uptake system in Escherichia coli upon hyper-osmotic stress at a low pH. *FEBS Lett* **447**: 144-148.

UniProt, C. (2023) UniProt: the Universal Protein Knowledgebase in 2023. *Nucleic Acids Res* **51**: D523-D531.

Untiet, V., Karunakaran, R., Kramer, M., Poole, P., Priefer, U., and Prell, J. (2013) ABC transport is inactivated by the PTS(Ntr) under potassium limitation in Rhizobium leguminosarum 3841. *PLoS One* **8**: e64682.

Valente, R.S., and Xavier, K.B. (2016) The Trk Potassium Transporter Is Required for RsmB-Mediated Activation of Virulence in the Phytopathogen Pectobacterium wasabiae. *J Bacteriol* **198**: 248-255.

Zakharyan, E., and Trchounian, A. (2001) K+ influx by Kup in Escherichia coli is accompanied by a decrease in H+ efflux. *FEMS Microbiol Lett* **204**: 61-64.

Zimmer, B., Hillmann, A., and Gorke, B. (2008) Requirements for the phosphorylation of the Escherichia coli EIIANtr protein in vivo. *FEMS Microbiol Lett* **286**: 96-102.

Figures

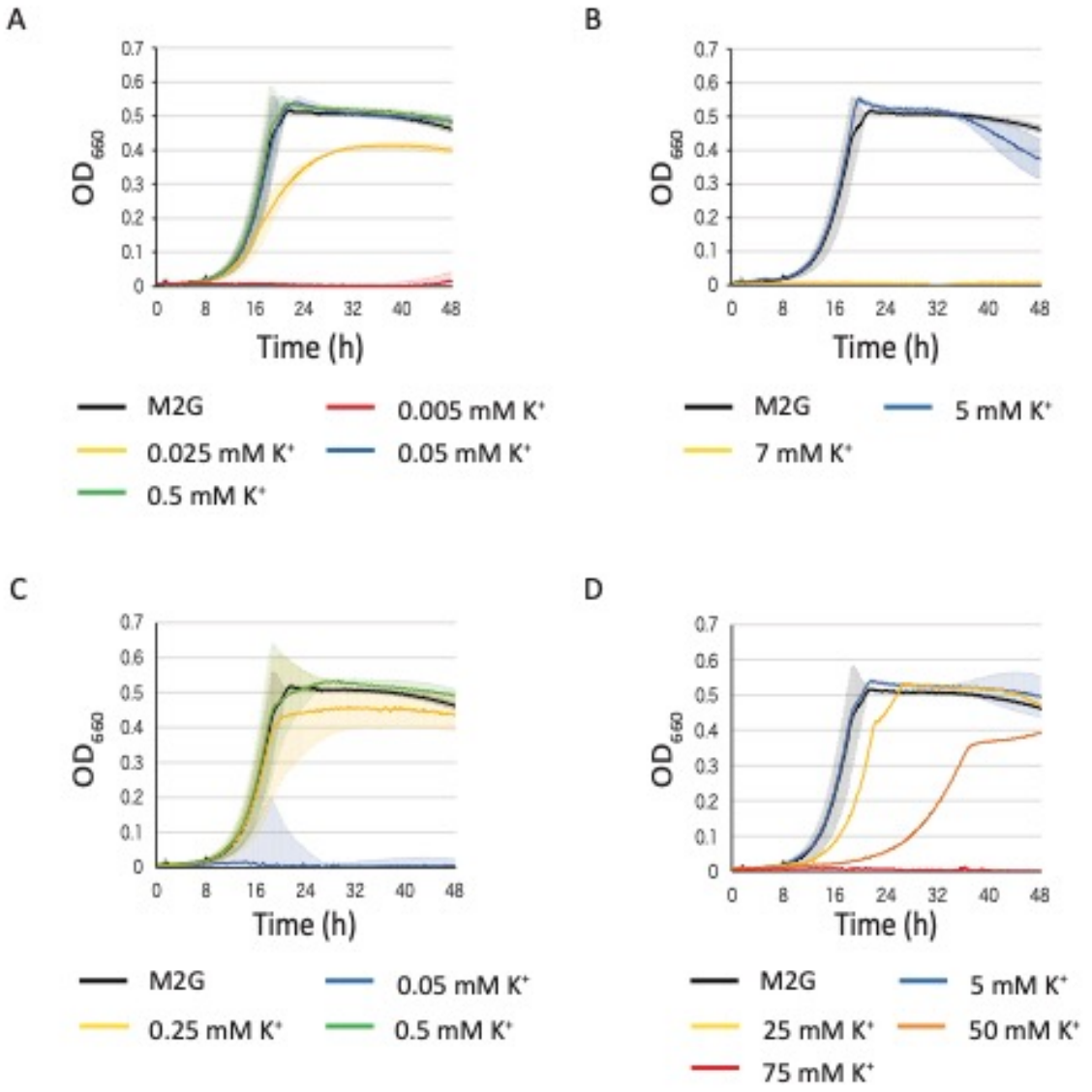

Figure 1. Impact of K^+ on *C. crescentus* growth. Growth of WT in M2G-K supplemented with different K^+ concentrations using K_2HPO_4 + KH_2PO_4 (A-B) and KCl (C-D) as K^+ source. Data represent average, n=3, and error bars= ±SD. Other concentrations tested are presented in Fig. S1.

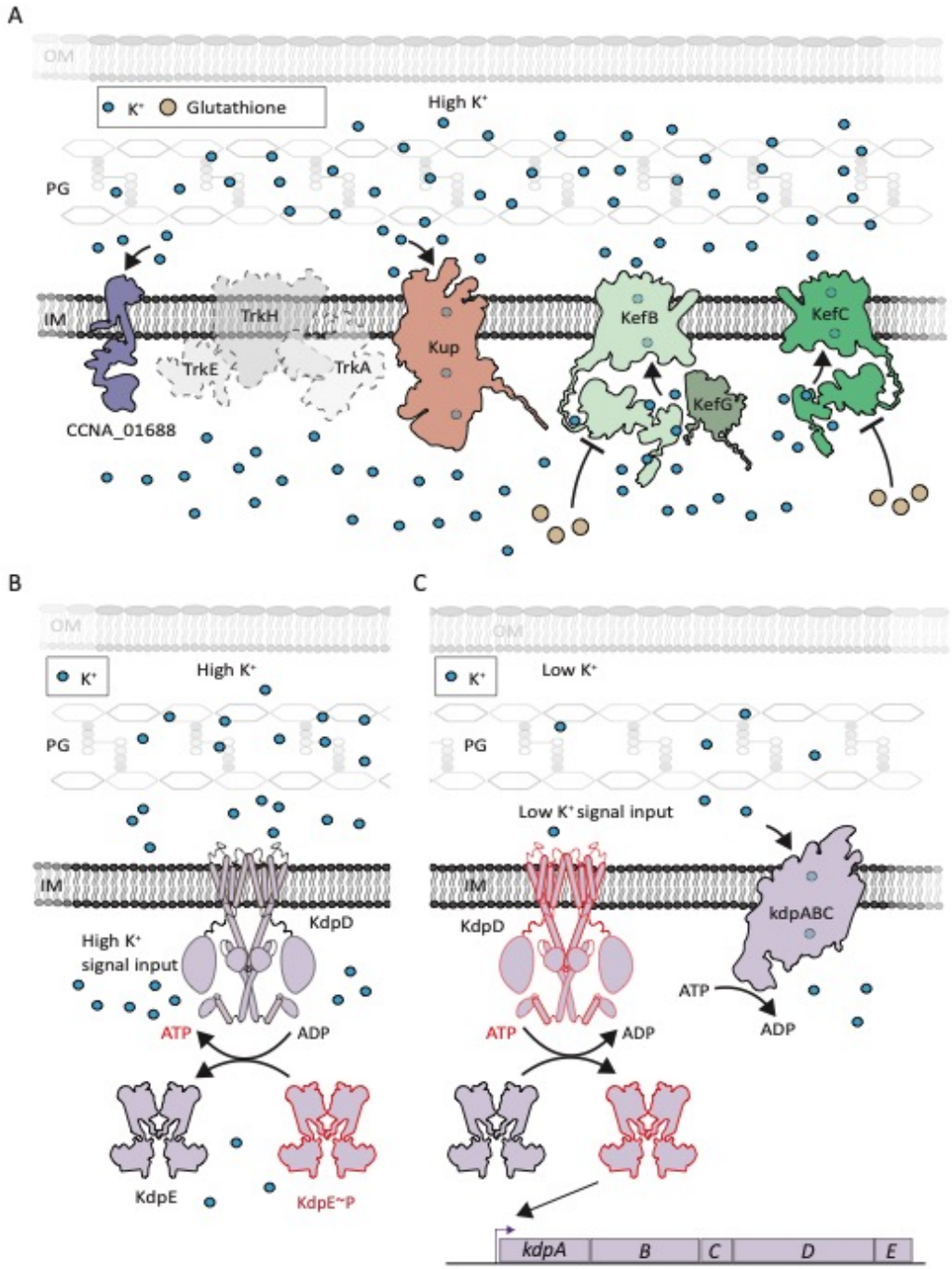

Figure 2. K^+ transport and response systems in Gram-negative bacteria. Schematic diagram of K^+-related proteins predicted to work at high (A-B) or low (C) K^+ concentrations. Coloured proteins correspond to the ones encoded in *C. crescentus* genome: CCNA_01688, Kup (CCNA_00130), KefB (CCNA_00204), KefG (CCNA_00205), KefC (CCNA_03611), KdpDE (CCNA_01666-CCNA_01667)

KdpFABC (CCNA_01662-CCNA_01665). The genes were identified using Biocyc collection of microbial genomes (Karp *et al.*, 2019) and structures of the proteins obtained using predictions with alphafold from Uniprot (UniProt, 2023). Outer Membrane (OM), peptidoglycan (PG), inner membrane (IM).

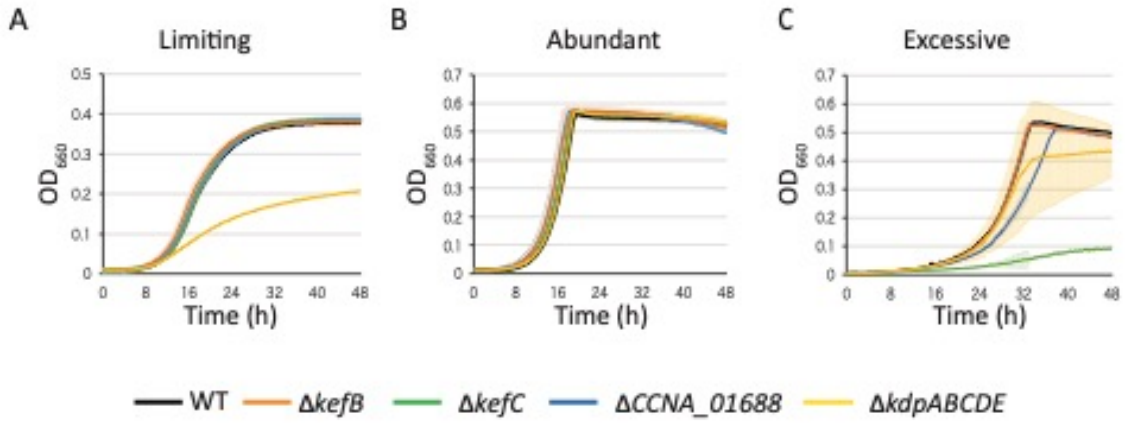

Figure 3. Deletion of K^+-related genes impact *C. crescentus* growth. Growth of WT, Δ*kefB*, Δ*kefC*, ΔCCNA_01688 and Δ*kdpABCDE* mutants in minimal media M2G-K supplemented with (A) limiting (0.025 mM), (B) abundant (0.5 mM) and (C) excessive (50 mM) K^+ concentrations. Data represent average, n=3, and error bars= ±SD.

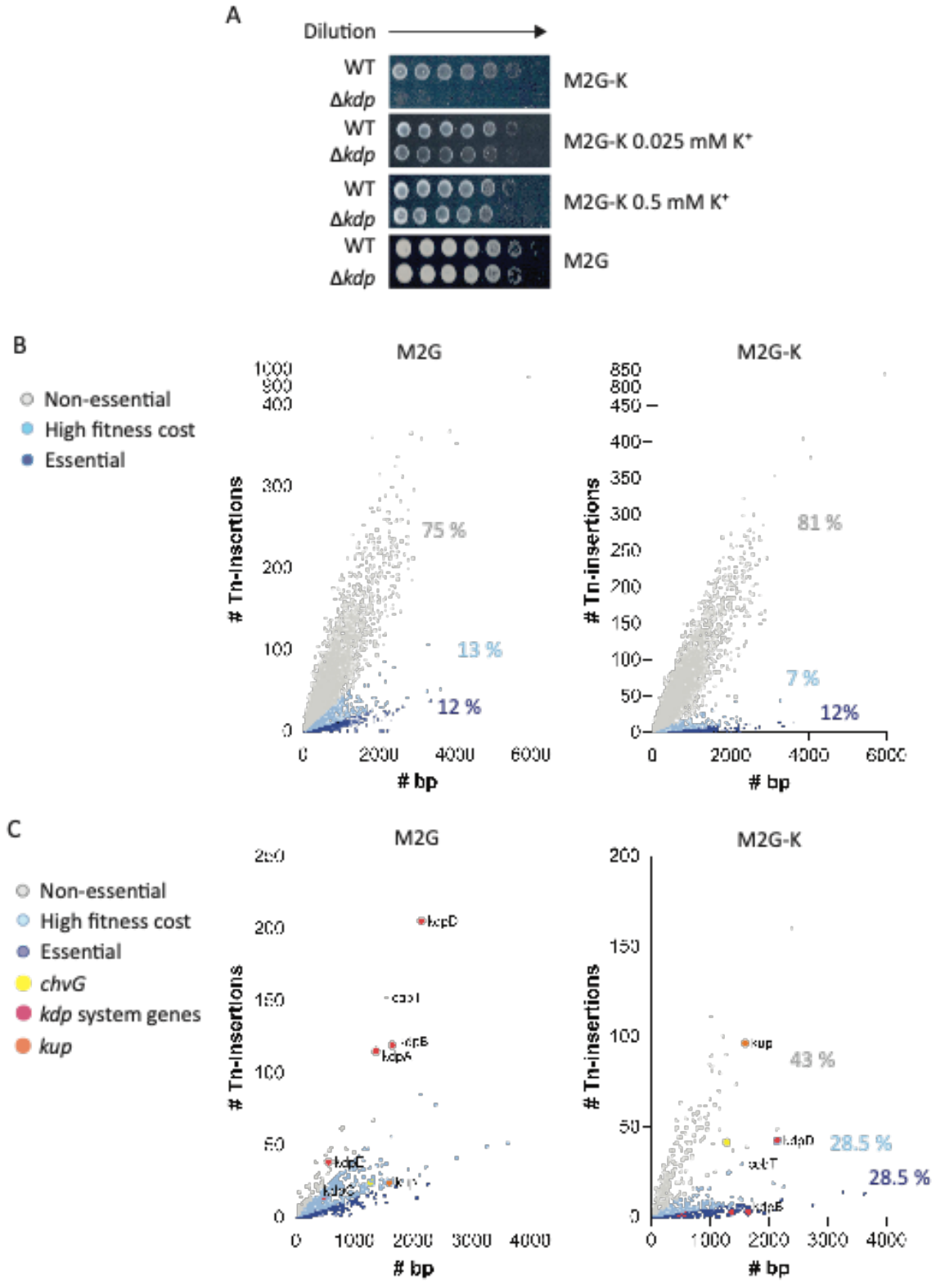

1033

1034 **Figure 4. Tn-seq and RNA-seq profile of *C. crescentus* cells in limiting K⁺**

1035 **conditions.** (A) Growth of WT and Δ*kdp* cells in M2G-K plates without or

supplemented with K^+. (B) Number of Transposon-insertions (#Tn-insertions) against the length (#bp) of 4186 genes in M2G and M2G-K media. Non-essential genes are highlighted in grey, high-fitness cost genes in light blue, and essential in dark blue. (C) Representation of genes that changed in their fitness-cost categories according to analysis done in M2G and M2G-K (B). (B-C) The percentage of genes in each category is indicated following the colour code.

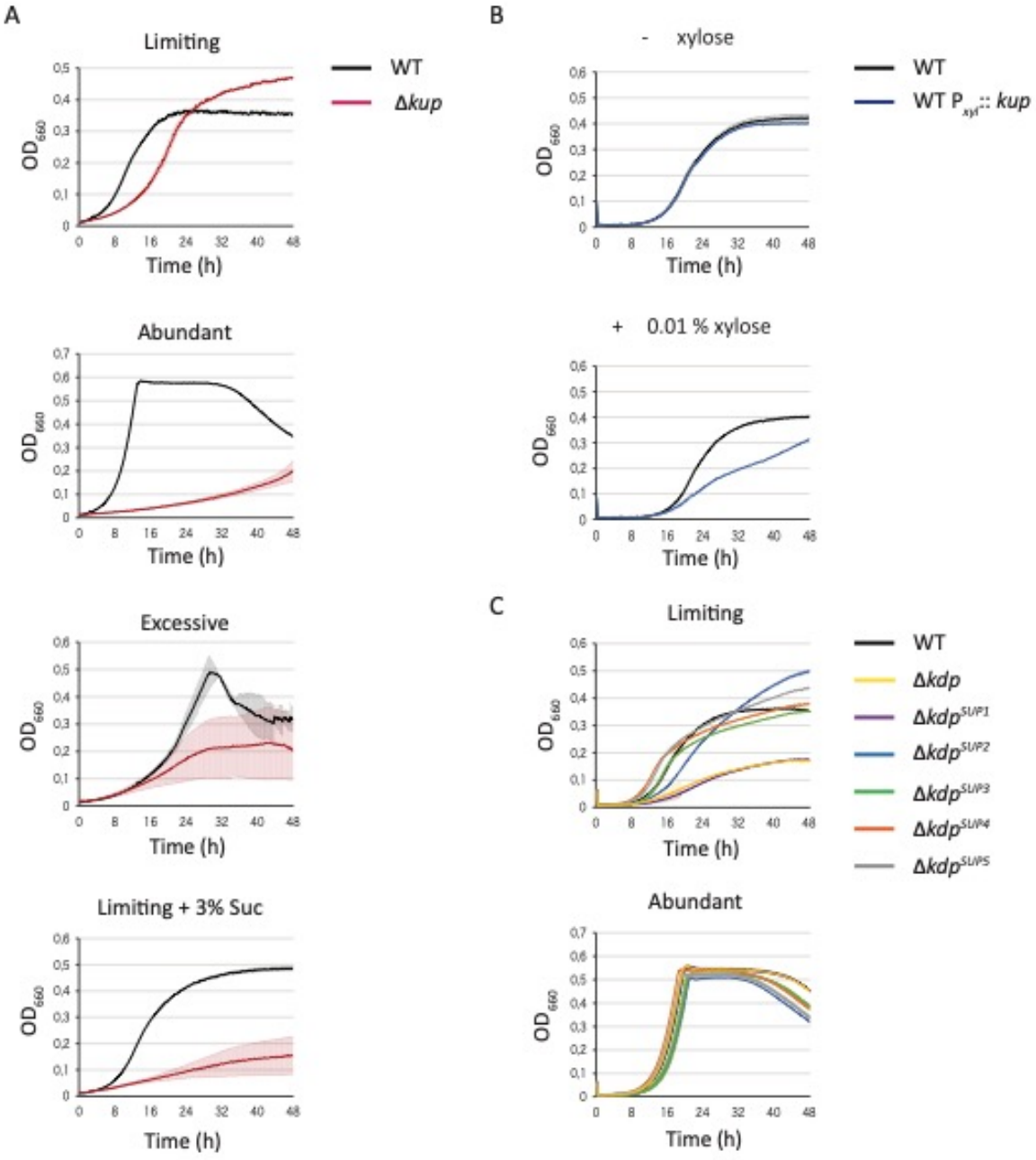

Figure 5. Impact of deletion and overexpression of the *kup* gene. (A) Growth of WT and Δ*kup* mutant in minimal media M2G-K supplemented with limiting (0.025 mM), abundant (0.5 mM), excessive (50 mM) K^+ concentrations or limiting (0.025 mM) K^+ concentrations and 3% sucrose. (B) Growth of WT expressing *kup* under xylose induction. (C) Growth of WT, Δ*kdp* and Δ*kdp* suppressors (Δ*kdp*^{SUP}) in minimal media M2G-K supplemented with limiting (0.025 mM) or abundant (0.5 mM). Data represent average, n=3, and error bars= ±SD.

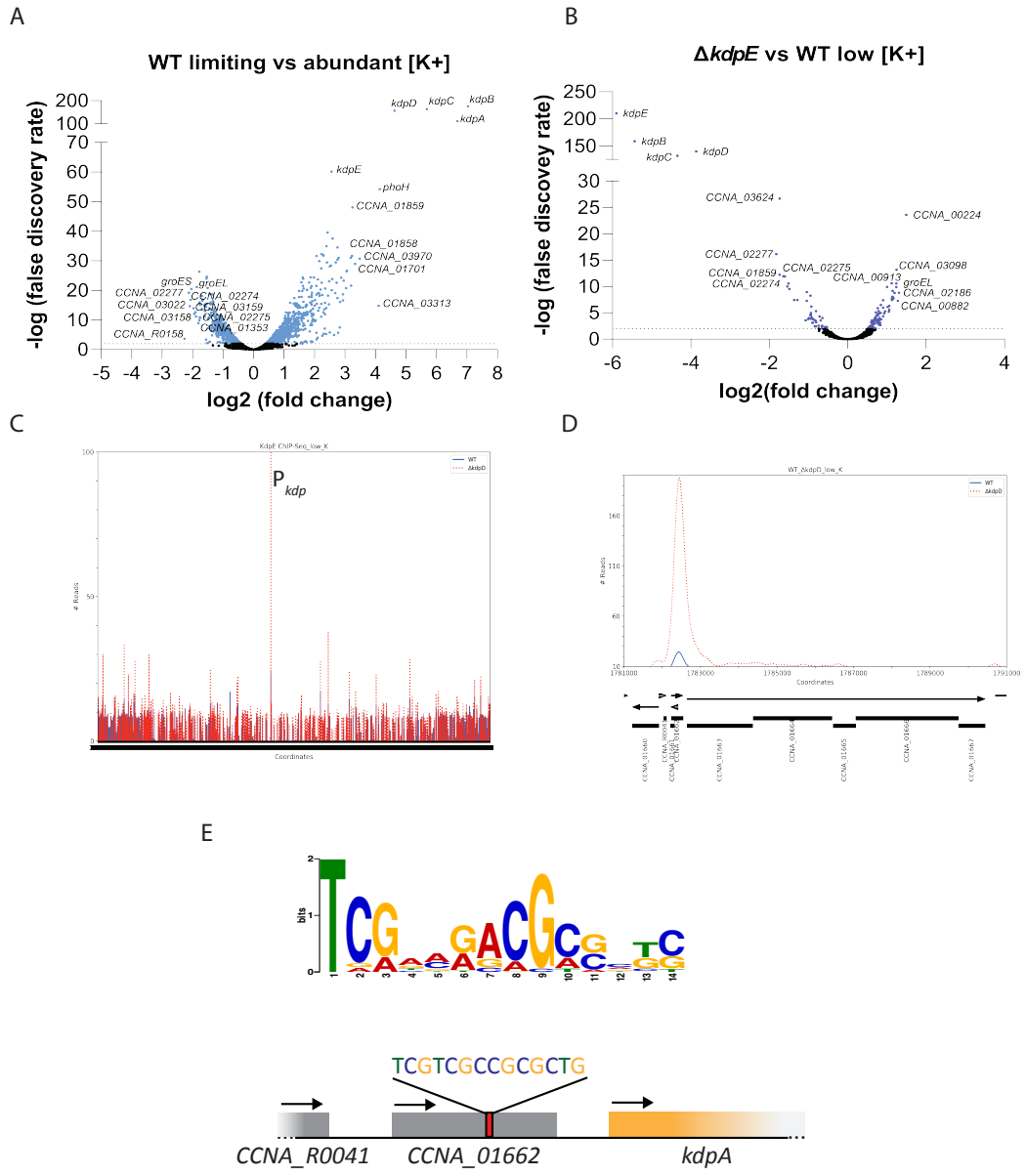

Figure 6. K^+ and KdpE-dependent regulon. (A-B) Volcano plots representing the relation between the log_2 fold change (FC) and -log False Discovery Rate (FDR) on gene expression between (A) WT in limiting *vs* abundant K^+ condition, and (B) Δ*kdpE* vs WT in limiting K^+ condition. Genes identified are presented as dots. Significant down- and up-regulated genes are presented as blue (A) and purple (B) dots, while genes with no significant alterations are presented as black dots. Top 10 down and upregulated genes are highlighted for each analysis. (C) Genome-wide occupancy of KdpE on the chromosome of *C. crescentus* determined by ChIP-seq on Δ*kdpE* P_{xylX}::*kdpE* Δ*xylX* and Δ*kdpDE* P_{xylX}::*kdpE* Δ*xylX*. The x-axis represents the coordinates on the genome (Mb), the y-axis shows the normalized ChIP-Seq read abundance in reads. The promoter region of *kdp* is highlighted. (D) Occupancy of KdpE on the *kdp* promoter Δ*kdpE* P_{xylX}::*kdpE* Δ*xylX* and Δ*kdpDE* P_{xylX}::*kdpE* Δ*xylX*. (E) WebLogo of predicted KdpE consensus sequence obtained with MEME and identification (with a *p-value* 7.71×10^{-5}) of the DNA binding sequence upstream of *kdpA*. Arrows indicate gene orientation for expression.

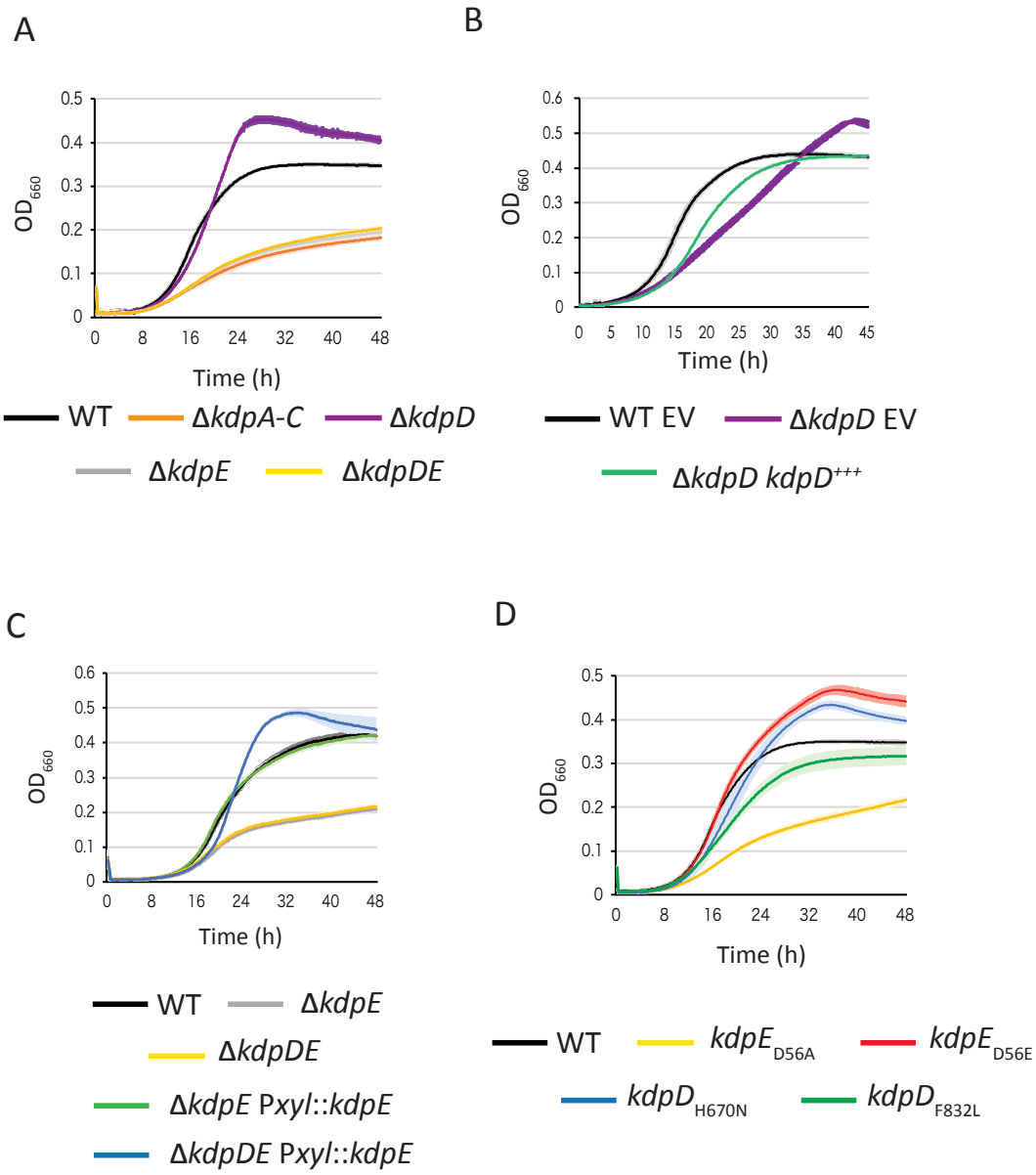

1066

1067 **Figure 7. KdpD downregulates KdpE to control growth in low K^+.** (A) Growth of
1068 WT, Δ*kdpABC,* Δ*kdpD*, Δ*kdpE* and Δ*kdpDE*. (B) Growth of WT and Δ*kdpD* carrying
1069 either pMR10 empty vectors (EV) or pMR10 P_{kdp}::*kdpD*. (C) Growth of WT, Δ*kdpE*,
1070 Δ*kdpDE* expressing *kdpE* from the *xylX* locus (P_{xylX}::*kdpE*). (D) Growth of *kdpD* and
1071 *kdpE* catalytic point mutants. Growth was done in minimal media M2G-K
1072 supplemented with limiting (0.025 mM) K^+ concentrations (A-D), media was
1073 additionally supplemented tetracycline for plasmid selection (B) or with 0.01 % xylose

1074 for the induction of *kdpE* expression (C). Data represent average, n=3, and error bars=

1075 ±SD.

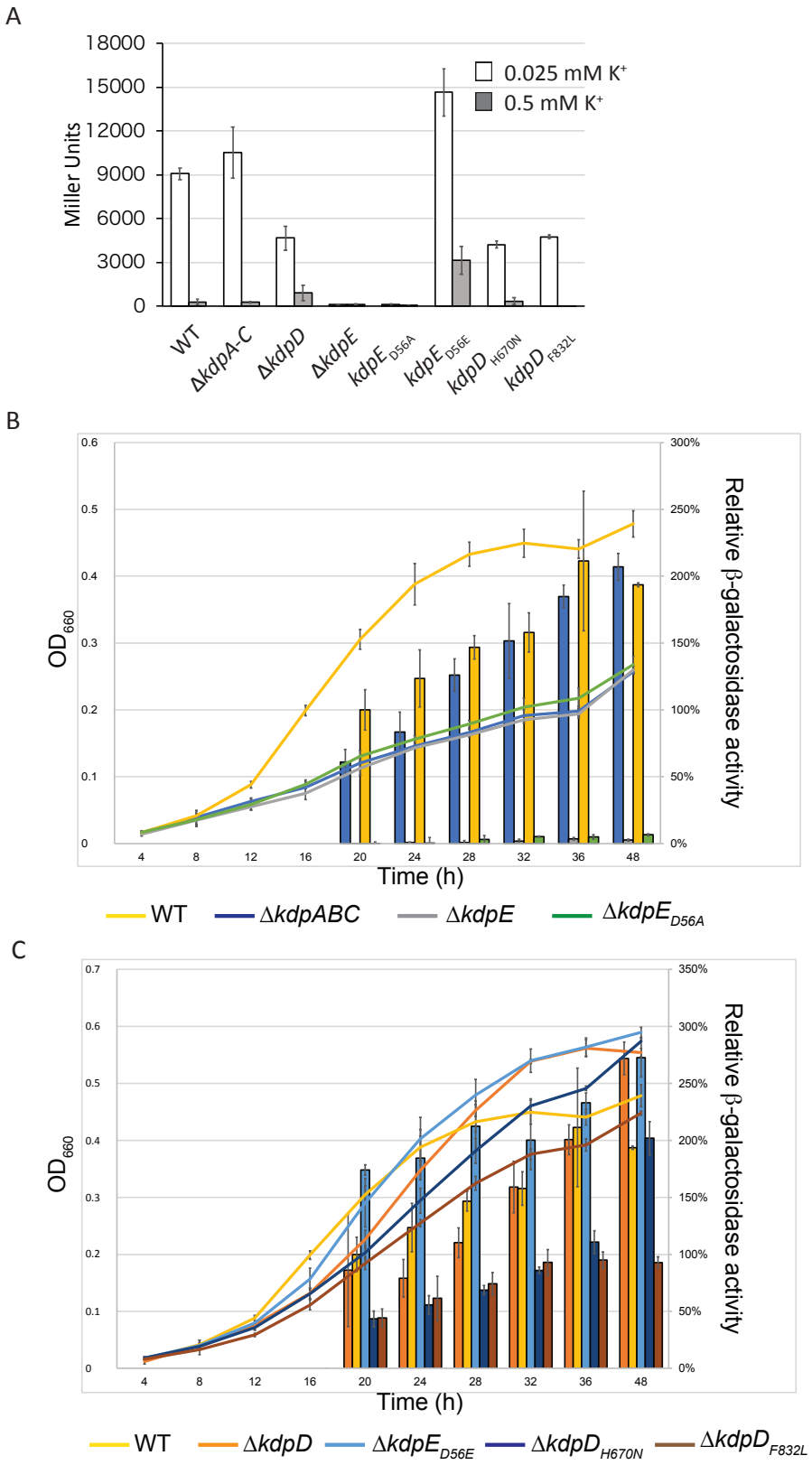

1076

Figure 8. Regulation of *kdp* expression (A) β-Galactosidase activities of WT and *kdp* mutants carrying a transcriptional P_{kdp}::*lacZ* fusion grown in M2G-K supplemented with limiting (0.025 mM) or abundant (0.5 mM). β-Galactosidase activities of WT and *kdp* mutants carrying a transcriptional P_{kdp}::*lacZ* fusion along the growth in M2G-K supplemented with limiting (0.025 mM). Statistical analyses were carried out via single factor ANOVA. Data represent average, n=3, and error bars= ±SD.